Article:

Gedalin, M., Balikhin, M. and Krasnoselskikh, V. (2026) Collisionless shocks: contemporary state after three quarters of a century of research. Reviews of Geophysics, 64 (3). e2025RG000893. ISSN: 8755-1209

https://doi.org/10.1029/2025rg000893

AGU ADVANCING EARTH AND SPACE SCIENCES

Reviews of Geophysics

REVIEW ARTICLE
10.1029/2025RG000893

Collisionless Shocks: Contemporary State After Three Quarters of a Century of Research

M. Gedalin[1], M. Balikhin[2,†], and V. Krasnoselskikh[3]

[1]Department of Physics, Ben-Gurion University of the Negev, Beer-Sheva, Israel, [2]ACSE, University of Sheffield, Sheffield, UK, [3]LPC2E/CNRS, Orleans, France

[†]Deceased 26 October 2025

Key Points:

- Subcritical shock structure and ion dynamics are well understood
- Qualitative understanding of the major features of supercritical quasiperpendicular shocks is achieved
- Quasiparallel shock structure and turbulent shocks are under active studies

Correspondence to:
M. Gedalin,
gedalin@bgu.ac.il

Citation:
Gedalin, M., Balikhin, M., & Krasnoselskikh, V. (2026). Collisionless shocks: Contemporary state after three quarters of a century of research. *Reviews of Geophysics*, *64*, e2025RG000893. https://doi.org/10.1029/2025RG000893

Received 5 FEB 2026
Accepted 24 JUN 2026

Author Contributions:
Conceptualization: M. Gedalin, M. Balikhin, V. Krasnoselskikh
Formal analysis: M. Gedalin, M. Balikhin, V. Krasnoselskikh
Investigation: M. Gedalin
Methodology: M. Gedalin, M. Balikhin, V. Krasnoselskikh
Validation: M. Gedalin, V. Krasnoselskikh
Visualization: M. Gedalin
Writing – original draft: M. Gedalin
Writing – review & editing: V. Krasnoselskikh

Abstract The collisionless shock research started in the late 1950s. Since then, plenty of data have been accumulated due to the large number of missions in the heliosphere, providing in situ measurements of the fields and particles. The quality of these measurements has vastly improved, especially in the last two decades. Much more data is available for analysis than is already analyzed. Theoretical studies received a push in 1966, when it was shown that shocks are formed due to the interplay between the nonlinear steepening and dispersive broadening of the magnetic field profile. At present, it is a common point of view that shocks are essentially shaped by the kinetics of ions. So far, we achieved a good semi-quantitative understanding of the ion heating in low-Mach number shocks and the relation of this process to the magnetic profile, and a qualitative understanding of the ion reflection and the nature of the well-structured magnetic field. Rippled and nonstationary quasi-perpendicular shocks have been observed, and theory is being developed.

Plain Language Summary Collisionless shocks are one of the most ubiquitous phenomena in space plasmas. They are found in the solar system and in far astrophysical objects. They are extremely efficient accelerators of charged particles. Understanding the structure of these shocks, in particular, how the increasing magnetic field behaves at the shock front, is important for understanding the whole spectrum of the processes at shocks and in space plasmas, in general. Astrophysical shocks can be observed only remotely, by electromagnetic radiation coming from the heated and accelerated particles. In the solar system, the electromagnetic fields and charged particles are directly measured by a number of missions. These in situ observations allowed us to substantially advance our knowledge of the shock physics. Shocks are characterized by their Mach number, which reaches the values of tens in the heliosphere, but may be around a thousand in astrophysical shocks. At present, we understand quite well the structure and processes at low Mach numbers, and only qualitatively the behavior of high Mach number shocks. The theory of the interaction of the fields and particles at such shocks is under active development.

1. Fundamental Processes in Space Plasmas and the Role of Collisionless Shocks

Collisionless shocks are one of the most ubiquitous phenomena in space plasmas. They are found in the laboratory setups (see, e.g., Schaeffer et al., 2015), at scales of $10^{-1}-10^{1}$ cm. Most of the shocks have been observed in the heliosphere at scales $\sim 10^{-1}-10^{2}$ AU. The most famous collisionless shocks reside in supernova remnants (SNR) and scales of several pc (Vink, 2004). The largest collisionless shocks are the galaxy cluster shocks (de Gasperin et al., 2022; Markevitch & Vikhlinin, 2007), having sizes of $\sim 10^{6}$ pc.

A collisionless shock is, albeit not a unique one, one of the most prominent space plasma systems built due to the strongly nonlinear interaction between the charged particles and the electromagnetic fields. One of the most important signatures of a shock is that there is a continuous flow of mass, momentum, and energy across the shock transition, accompanied by entropy production. The manifestation of the conservation laws, requiring the equality of the fluxes in the upstream region, from which the plasma flows into the shock, and the downstream region, into which the plasma proceeds after having been processed (modified) by the shock, are the so-called Rankine-Hugoniot relations, establishing the connection between the upstream and downstream shock parameters.

The major role of the above-mentioned collisionless shocks, as viewed in the shock frame, is the redistribution of the energy of the directed flow into the energy of heated ions and electrons, the energy of the enhanced magnetic field, and the energy of a small fraction of particles accelerated to high energies. Cosmic rays with energies up to 10^{15} eV are widely believed to be produced by the galactic SNR shocks (Marcowith et al., 2016). Higher energies, up to 10^{18} eV and possibly above, probably can be achieved by further acceleration at galaxy cluster shocks

(Ptuskin et al., 2009). The acceleration efficiency of the collisionless shocks is the main reason for unfading interest in shock physics.

A collisionless shock is a profoundly multiscale structure. The electron distribution is affected by the fields at spatial scales substantially smaller than the shock transition width. The ion distributions and the magnetic profile are modified at the scale of the shock transition, while particle acceleration occurs at a much larger scale via the diffusive shock acceleration (DSA) mechanism (Axford et al., 1977; Blandford & Eichler, 1987; Blandford & Ostriker, 1978; Drury, 1983; Krymskii, 1977; Toptyghin, 1980). While the smallest scale fields are related to the electron dynamics, the magnetic profile of the shock front, often referred to as the shock structure, is formed by interaction of the macroscopic magnetic and electric field with the thermal and weakly superthermal ions. Although the spatial scale at which DSA works is much larger than the scale of the shock structure, the latter plays an important role in establishing the connection (matching) between the upstream and downstream distributions of accelerated particles and thus determining the energy spectrum of the distribution of these particles.

2. Historical Remarks

A shock is originally a hydrodynamical (HD) concept, where it is a planar, standing discontinuity through which a fluid flows and at which the velocity drops, while the density and temperature increase. The concept was generalized in magnetohydrodynamics (MHD), where the magnetic field change also occurs while the tangential component of the electric field is continuous (de Hoffmann & Teller, 1950). In HD, a shock occurs when the velocity along the shock normal drops from a supersonic velocity in the upstream region (plasma flows into the discontinuity) to a subsonic velocity (plasma flows out of the discontinuity). In MHD, there are three characteristic speeds of propagating waves and two types of shocks: fast shocks, in which the velocity drops from above the fast magnetosonic speed to below it, and the magnetic field increases, and slow shocks, in which the velocity crosses the slow magnetosonic speed and the magnetic field decreases. The present review addresses fast shocks.

The beginning of the collisionless shock studies occurred in an explosive way. Thomas Gold predicted in 1955 that the space between the Sun and Earth must be filled with plasma and that shocks should be able to propagate in this plasma. Shortly after that, the existence of the solar wind and its features were theoretically predicted (Parker, 1958). Almost immediately, a collisionless shock was produced in a lab experiment (Patrick, 1959), and the first theoretical works on the shock structure were published (Adlam & Allen, 1958; Davis et al., 1958; Gardner et al., 1958; Sagdeev, 1958). On the basis of rhe plasma and magnetic field measurements in 1961–1962, the existence of the Earth bow shock was predicted (Axford, 1962; Kellogg, 1962). This shock was observed shortly (Ness et al., 1964), together with more lab produced shocks (Paul et al., 1965).

An MHD shock is a zero-width discontinuity at which the magnetic field jumps. In observed shocks, the magnetic field increase occurs continuously at a finite spatial length shock transition region. In a collisional shock dominated by Coulomb collisions, the magnetic profile would always be monotonic. The vast majority of shocks in space occur in plasmas where the mean free path of Coulomb collisions greatly exceeds the width of the shock transition. The magnetic field profile of a collisionless shock is not necessarily monotonic, and one of the central problems of the shock physics has always been explanation of the shock structure and the mechanism of its formation (Davis et al., 1958; Fishman et al., 1960; Marshall, 1956; Sagdeev, 1966; Sen, 1956; Tidman, 1958).

2.1. Early Models

The theoretical approach to the studies of the shock structure was initiated by the two-fluid analysis of a nonlinear magnetosonic wave, propagating perpendicularly to the ambient magnetic field (Adlam & Allen, 1958; Davis et al., 1958; Gardner et al., 1958; Sagdeev, 1958). The approach was further developed to elucidate the interplay between the nonlinear steepening and dispersive broadening of a large-amplitude magnetosonic wave (Sagdeev, 1966). It was shown that this wave is negatively dispersive, $\omega = kv_F(1 - k^2 l_d^2)$, and described by a pseudopotential-type differential equation, which admits a soliton solution. The soliton width is determined by the dispersive length l_d, which is the electron inertia length for the perpendicular propagation. If a weak dissipation is present, instead of a soliton, we expect to get a shock-like solution with large downstream magnetic oscillations. The spatial period of the oscillations is determined by the dispersive length, while the much larger spatial size on which the oscillations damp is determined by the dissipation. It was suggested that there is a maximum Mach number of a nonlinear soliton, beyond which ions begin to be reflected, causing effective dissipation

(Sagdeev, 1966, 1979; Sagdeev & Kennel, 1991). This approach remains in the basis of the modern theoretical studies magnetized collisionless shocks.

The approach was further extended onto positively dispersive oblique magnetosonic waves where an upstream precursor develops (Kennel & Sagdeev, 1967). At the same time, MHD with various dissipation mechanisms (resistivity, heat conduction, viscosity) was analyzed (Coroniti, 1970; Kennel, 1988). The concept of the first critical Mach number emerged, above which resistivity and heat conduction are unable to maintain a stable shock.

Analytical studies of planar stationary structures within the two-fluid approach with resistivity included allowed establishing the relation between the two tangential components of the magnetic field and the spatial scale of the precursor oscillations and the ramp width (see, e.g. Gedalin, Kushinsky, & Balikhin, 2015, and references therein). At the ramp and behind it, ion kinetics becomes essential. The equations of ion motion in the shock fields are not integrable. Further theoretical studies have been performed using test particle analysis in a model shock front. These studies revealed the role of the kinematic collisionless relaxation (Balikhin et al., 2008; Gedalin, 2019b, 2019c; Gedalin, Friedman, & Balikhin, 2015) and the relation of the downstream magnetic oscillations to the quasi-periodic variations of pressure of the non-gyrotropic ion distribution. The test particle analyses are not self-consistent. Self-consistent simulations evolved from 1D hybrid simulations to 2D PIC simulations. Simulations would require a separate long review and are not covered here.

2.2. Observations

The progress in shock observations has been more impressive than the progress in the theory of the shock structure. A large number of missions have investigated and are investigating the Earth bow shock: from IMP 1 and Vela 4 to dual ISEE 1/ISEE 2 and AMPTE-UKS/AMPTE-IRM to multi-spacecraft Cluster, THEMIS, and MMS. A number of missions have observed shocks at inner and outer planets: MESSENGER at Mercury, Venus Express at Venus, MAVEN at Mars, Cassini at Saturn. Interplanetary shocks have been observed by Wind, STEREO, and Artemis at 1 AU. The termination shock was crossed by Voyager. Near Sun shocks are being observed by the Solar Orbiter and Parker Solar Probe. The above list is incomplete and is brought to show that much more data has been and is being accumulated than can be analyzed at the same rate. The quality of measurements, especially the temporal resolution, is constantly improving, so that often the already available vast amount of data remains untouched while the new data is preferred. Yet, important steps in the shock studies were done using very early observations. The laminar profiles of low-Mach number low-β shocks (Greenstadt et al., 1975), as well as complex magnetic profiles of high-Mach number high-β shocks (Formisano et al., 1975) were revealed by exploring OGO 5 observations with the resolution 0.144 s/sample. The dual spacecraft ISEE 1 and 2 measured 6 magnetic field vectors per second and full ion and electron distributions every 3 s. Availability of two spacecraft simultaneous measurements allowed statistical analysis of the widths of laminar shocks (Russell, Hoppe, Livesey, Gosling, & Bame, 1982). The high resolution of the particle measurements spurred studies of ion gyration and reflection in the shock front (Paschmann et al., 1982) and provided detailed information about the evolution of the ion distribution across the shock (Sckopke et al., 1983). A "typical" profile of a high-Mach number shock was deduced from ISEE observations (Scudder et al., 1986). ISEE lifetime was substantially larger than that of OGO and IMP 1/Explorer 18, so that statistical analyses of the shock features, like the overshoot strength (Livesey et al., 1982) or the ramp width (Newbury et al., 1998) could be performed.

2.3. First Multipoint Measurements: Waves or Macroscopic Fields

Four-spacecraft observations (ISEE 1, 2, 3, and IMP 8) have been used for the determination of the interplanetary shock normals (Russell & Alexander, 1984; Russell et al., 1983) long ago. Similarly, multipoint observations were used for the analysis of waves upstream of interplanetary shocks (Russell, 1988; Russell et al., 1987). The multi-spacecraft missions with small separations, Cluster, THEMIS, and MMS, allowed determination of the shock normal and speed using multipoint measurements at the terrestrial bow shock. Rippling (Gingell et al., 2017; Hanson et al., 2019; Johlander et al., 2016; Lobzin et al., 2008; Lowe & Burgess, 2003) and reformation (Dimmock et al., 2019; Lefebvre et al., 2009; Liu et al., 2021; Lobzin et al., 2007; Turner et al., 2021) are often identified by multipoint measurements.

Table 1
Time-Resolution of the Fields and Full Distribution Measurements

Mission	Magnetic field	Electric field	Plasma
Wind: MFI (Lepping et al., 1995), SWE (Ogilvie et al., 1995)	11 or 22 Hz	No	1 s
ACE: MAG (Smith et al., 1998), SWEPAM (McComas et al., 1998)	3–6 Hz	No	64 s
STEREO: IMPACT (Luhmann et al., 2008; Acuña et al., 2008), PLASTIC (Galvin et al., 2008)	32 Hz	No	1 min
Cluster: FGM (Balogh et al., 2001), EFW (Gustafsson et al., 2001), CIS (Rème et al., 2001)	22 Hz (67 Hz in burst mode)	450 Hz (burst mode)	4 s
THEMIS: FGM (Auster et al., 2008), EFI (Bonnell et al., 2008), ESA (McFadden et al., 2008)	64 Hz	DC up to 4 kHz	3 s
MMS: FGM (Russell et al., 2016), SPD-ADP (Ergun et al., 2016; Lindqvist et al., 2016), FPI (Pollock et al., 2016)	128 Hz (survey), 8,192 Hz (burst)	up to 16,384 Hz	30 ms
SOLO: MAG (Horbury et al., 2020), RPW (Maksimovic et al., 2020), SWA (Owen et al., 2020)	16–128 Hz	<10 kHz	3 s, 0.125 s (burst)
PSP: FIELDS (Bale et al., 2016; Malaspina et al., 2016), SWEAP (Kasper et al., 2016)	128 Hz	DC to 60 kHz	∼1 s

2.4. Contemporary Observations

Table 1 summarizes the capabilities of various contemporary missions. At collisionless shocks, the magnetic field, the electric field, and the velocity distributions of various species are measured by the spacecraft. Not all spacecraft measure all fields or particle distributions. All measurements are performed in the spacecraft frame, and every variable is measured as a function of time. Deducing spatial dependence requires the knowledge of the spacecraft velocity relative to the shock, at the very least. The better the temporal resolution of the measurements, the more information is collected. High sampling rates alone, however, do not ensure that detailed information is obtained. The effective resolution (not the nominal one) also depends on the physical scales of the shock features and the shock speed in the spacecraft frame. The latter is low for the nearly standing Earth bow shock and high for traveling interplanetary shocks. The Earth bow shock is typically a high-Mach number, $M_A > 5$, shock (Gedalin et al., 2021; Scudder et al., 1986). Interplanetary shocks are typically low-Mach number, $M_A \lesssim 3$, shocks (Neugebauer, 2013), although high-Mach number shocks have been recently observed closer to the Sun (Dimmock et al., 2023; Jebaraj, Agapitov, Krasnoselskikh, et al., 2024).

3. Shock Structure: Current State of Art

3.1. Conservation Laws

Whatever happens in the shock transition, the general conservation laws must be maintained. In what follows, we restrict ourselves to the majority of the heliospheric shocks, where the radiation losses are negligible, the interaction with neutrals (charge exchange) is negligible (except for the termination shock), and the composition changes are negligible. In these shocks, the mass conservation means conservation of the number of particles of each species separately. The momentum conservation and the energy conservation include all species and the magnetic field as well, the latter as the electromagnetic stress tensor and Poynting vector. In non-relativistic shocks, the displacement current and the electric field energy are also negligible when integrated or averaged over typical electron temporal and spatial scales, because the shock structure refers to the ion scales. In addition, the induction equation must be valid throughout. In order to make the further discussion more specific, we shall define the coordinates so that the normal $\hat{n}$ to the MHD shock discontinuity is along the x-axis, $\hat{n} = \hat{x}$. We shall work in the shock frame where the plasma flows and the shock stands. The Normal Incidence Frame (NIF) is the frame in which the upstream ($x < 0$ far from the shock, subscript u) flow velocity is along the shock normal, $\boldsymbol{V}_u = V_u\hat{x}$. The other coordinates are chosen so that in the upstream region (assumed uniform), the magnetic field is $\boldsymbol{B}_u = B_u(\cos\theta_{Bn}, 0, \sin\theta_{Bn})$. The angle $\theta_{Bn} = \widehat{\boldsymbol{B}_u\hat{n}}$ is referred to as the shock angle and is one of the main shock parameters. Shocks are called quasi-perpendicular, if $|90° - \theta_{Bn}| < 45°$, and quasi-parallel otherwise. Note that this definition is more general than the one typically used, to take into account that $\cos\theta_{Bn}$ is not necessarily positive, that is, while the shock normal points toward downstream, the magnetic field vector may point toward upstream. Shocks with $80^\circ > |90^\circ - \theta_{Bn}| > 10^\circ$ are often referred to as oblique shocks, while those with $|90^\circ - \theta_{Bn}| < 10^\circ$ are nearly-perpendicular, and those with $|90^\circ - \theta_{Bn}| > 80^\circ$ are nearly-parallel. The coplanarity theorem states that in the uniform downstream region ($x > 0$ far from the shock, subscript d), the magnetic field is $\boldsymbol{B}_d = B_d(\cos\theta_d, 0, \sin\theta_d)$. The ratio B_d/B_u will be referred to as the magnetic compression ratio, and the electrodynamics imposes the constraint $B_u \cos\theta_{Bn} = B_d \cos\theta_d$. The downstream plasma velocity is also in the $x - z$ plane, $\boldsymbol{V}_d = (V_{dx}, 0, V_{dz})$. With this choice of the coordinates and NIF, the electric field is

$$\boldsymbol{E}_u = -\frac{\boldsymbol{V}_u \times \boldsymbol{B}_u}{c} = \left(0, \frac{V_u B_u \sin\theta_{Bn}}{c}, 0\right) = \boldsymbol{E}_d = -\frac{\boldsymbol{V}_d \times \boldsymbol{B}_d}{c} \tag{1}$$

In the standard approach, the fluxes of the conserved quantities in both uniform asymptotic regions, upstream and downstream, must be equal:

$$n_s V_x = \text{const} \tag{2}$$

$$\sum_s (n_s m_s) V_x = \text{const} \tag{3}$$

$$\sum_s \left(n_s m_s V_x^2 + p_s\right) + \frac{B^2}{8\pi} = \text{const} \tag{4}$$

$$\sum_s n_s m_s V_x \boldsymbol{V}_{s\perp} - \frac{B_x \boldsymbol{B}_\perp}{4\pi} = \text{const} \tag{5}$$

$$\left(\sum_s \left(\frac{1}{2} n_s m_s V_x^2 + \epsilon_s + p_s\right) + \frac{B^2}{4\pi}\right) V_x - \frac{V_x(\boldsymbol{V}\cdot\boldsymbol{B})}{4\pi} = \text{const} \tag{6}$$

Here n_s is the number density of species s, m_s is the mass of the particle of species s, and p_s and ϵ_s are the kinetic pressure (assumed isotropic) and the energy density, respectively, of species s. The velocity V_x is assumed to be the same for all species. The upstream and downstream plasma are quasineutral and without currents:

$$\sum_s n_s q_s = 0, \qquad \sum_s n_s q_s \boldsymbol{V} = 0 \tag{7}$$

where q_s is the charge of the particle of species s, and all species are moving together in the asymptotic regions. Equations 1–6, usually written in terms of single fluid parameters, such as $\rho = \sum_s n_s m_s$, constitute the system of the Rankine-Hugoniot relations (RH) (see, e.g. Kennel et al., 1985) used for the derivation of the downstream plasma and magnetic field parameters from the upstream plasma parameters. The latter are the shock angle θ_{Bn}, the Alfvénic Mach number $M_A = V_u/v_A$, where $v_A^2 = B_u^2/4\pi\rho_u$, and $\beta = 8\pi\sum_s p_{su}/B_u^2$. The Alfvénic Mach number is often replaced with the fast magnetosonic Mach number $M_F = V_u/v_F$, where

$$\frac{v_F}{v_A} = \sqrt{\frac{1}{2}\left(1 + \beta\gamma/2 + \sqrt{(1+\beta\gamma/2)^2 - 2\beta\gamma\cos^2\theta_{Bn}}\right)} \tag{8}$$

γ being the adiabatic index. The fast speed and fast Mach number depend on the assumed equation of state, so in what follows we shall use the Alfvénic Mach number unless stated otherwise.

If a shock is planar and stationary the fluxes of mass, momentum, and energy must be constant throughout the shock and not only in the asymptotic upstream and downstream regions. At the shock crossing ion distributions become non-gyrotropic (Gedalin, 1996b; Li et al., 1995), and the above fluxes should be replaced with the moments of the distribution function $f(\boldsymbol{r}, t, \boldsymbol{v})$, as follows:

$$n(\boldsymbol{r},t) = \int f(\boldsymbol{r},t,\boldsymbol{v})d^3\boldsymbol{v} \tag{9}$$

$$n(\boldsymbol{r},t)\boldsymbol{V}(\boldsymbol{r},t) = \int \boldsymbol{v}f(\boldsymbol{r},t,\boldsymbol{v})d^3\boldsymbol{v} \tag{10}$$

$$P_{ij}(\boldsymbol{r},t) = m\int v_i v_j f(\boldsymbol{r},t,\boldsymbol{v})d^3\boldsymbol{v} = p_{ij} + \Pi_{ij} \tag{11}$$

$$p_{ij} = m\int (v_i - V_i)(v_j - V_j)f(\boldsymbol{r},t,\boldsymbol{v})d^3\boldsymbol{v}, \qquad \Pi_{ij} = nmV_iV_j, \tag{12}$$

$$\epsilon(\boldsymbol{r},t) = \frac{m}{2}\int (\boldsymbol{v}-\boldsymbol{V})^2 f(\boldsymbol{r},t,\boldsymbol{v})d^3\boldsymbol{v} \tag{13}$$

$$Q_{ijk} = m\int (v_i - V_i)(v_j - V_j)(v_k - V_k)f(\boldsymbol{r},t,\boldsymbol{v})d^3\boldsymbol{v} \tag{14}$$

The expressions (9–14) are written here in the most general way, for any spatially and temporally dependent distribution function of any species. Here P_{ij} is the total pressure, which includes the dynamic pressure Π_{ij} and the kinetic pressure p_{ij}, and Q_{ijk} is the heat flux. Then, in the most general form, the momentum and energy conservation have the form:

$$\frac{\partial}{\partial t}\left(\sum_s n_s m_s V_{s,i}\right) + \frac{\partial}{\partial x_j}\left(\sum_s P_{s,ij} + \frac{B^2\delta_{ij} - 2B_iB_j}{8\pi}\right) = 0 \tag{15}$$

$$\frac{\partial}{\partial t}\left(\left(\sum_s \frac{1}{2}n_s m_s \boldsymbol{V}_s^2 + \epsilon_s\right) + \frac{B^2}{8\pi}\right) + \frac{\partial}{\partial x_j}\left(\sum_s (P_{s,ij}V_{s,i} + Q_{s,iij}) + \frac{c}{4\pi}\epsilon_{jkl}E_kB_l\right) = 0 \tag{16}$$

At present, non-gyrotropy of the electron distribution, if any, cannot be resolved by observations at heliospheric shocks. If a shock is nearly planar and stationary, the time derivatives may be neglected and only the spatial derivative along the shock normal, $\partial/\partial x$, is of importance, so that the above differential relations reduce to algebraic constraints, similar to the standard RH but with non-gyrotropic ion pressure. For a rippled or just time-dependent shock, proper spatial and temporal averaging has to be done to arrive at a physically meaningful generalization of RH (Gedalin & Ganushkina, 2022). The presence of large-amplitude small-scale variations of the plasma density and velocity, and of the magnetic field, leads to an even more complicated form of the conservation laws for the properly averaged variables (Gedalin, 2023b, 2023c; Terasawa et al., 2007). In particular, the rms magnetic field $\sqrt{\langle B^2\rangle}$ may appear by an order of magnitude larger than the mean magnetic field magnitude $|\langle\boldsymbol{B}\rangle|$ (Golan & Gedalin, 2025).

3.2. Subcritical Shocks

It is widely accepted to categorize all shocks as either subcritical or supercritical. There are at least three different critical Mach numbers (Kennel, 1987; Kennel et al., 1985). The first critical Mach number M_{c1} corresponds to the maximum Mach number above which resistivity alone cannot maintain the shock profile, and is determined by the condition that the downstream sound speed begins to exceed the downstream velocity along the shock normal. The whistler critical Mach number M_{cw} is determined by the maximum Mach number at which the upstream whistler can stand in the shock frame. Lastly, the second critical Mach number M_{c2} is defined by the requirement that there will be a sufficient number of reflected ions. It is said to be determined by the condition that the downstream ion thermal speed begins to exceed the downstream velocity along the shock normal (Leroy et al., 1982). For $\theta_{Bn} = 60°$ and $\beta = 0.5$, the critical Mach numbers are estimated as $M_{c1} \approx 2$, $M_{cw} \approx 6$, and $M_{c2} \approx 3$ (Kennel et al., 1985). In the range of Mach numbers below M_{c1}, the shocks are "dissipative." In the range between M_{c1} and M_{cw} the shocks are "dispersive." Above M_{c2}, the shocks are dominated by reflected ions. Note that dispersive shocks may be reflection-dominated, according to this nomenclature. The critical Mach numbers are model-dependent since they are defined within one-fluid or two-fluid approaches, which contain

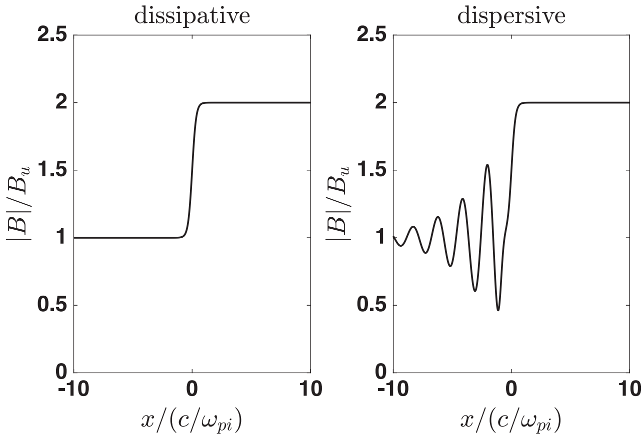

Figure 1. A schematic view of the magnetic field profile of a subcritical shock. (Left) A dissipative shock, $M < M_{c1}$. (Right) A dispersive shock, $M_{c1} < M < M_{cw}, M_{c2}$.

model equations of state. A more meaningful physical definition of criticality would be that reflected ions play an important role in supercritical shocks but are unimportant in subcritical shocks. This definition would not allow the calculation of the critical Mach number, and it does not even mean that there is a sharp transition from the subcritical regime to the supercritical regime. Indeed, ion reflection is not "switched on" abruptly when one or more shock parameters cross any threshold. Yet, it is possible to evaluate the reflected ion contribution to the pressure tensor.

Figure 1 schematically shows the expectations for the magnetic profile of a subcritical shock, in the dissipative and dispersive regimes. The whistler precursor in the right panel may be grossly exaggerated. The main conclusion of the early studies was that the main magnetic field jump, ramp, is followed by the asymptotic downstream magnetic field, at least for low β (Farris et al., 1993). The overshoot, that is, the post-ramp increase of the magnetic field above the far downstream value, was widely believed to be produced by the reflected ions in supercritical shocks. The ramp width is expected to be of the order of the ion inertial length, c/ω_{pi}, where $\omega_{pi} = \sqrt{4\pi n_u e^2/m_p}$.

Figure 2 shows profiles of observed subcritical shocks. The top left panel shows the magnetic profile of an interplanetary shock crossed by THEMIS C on 30 March 2011 at 08:09:40 UTC. The shock parameters are $M_A \approx 1.25$, $\theta_{Bn} \approx 70°$, and $\beta \approx 0.08$ (Pope et al., 2018). The profile has an apparently standing whistler precursor, an overshoot, and downstream magnetic oscillations.

The bottom left panel is a rare example of a subcritical terrestrial bow shock crossed by MMS 1 on 24 April 2023 at 04:15:25 UTC. The parameters are $M_A \approx 1.5$, $\theta_{Bn} \approx 68°$, and $\beta \approx 0.035$ (Graham & Khotyaintsev, 2025). The precursor is barely seen. The overshoot and downstream oscillations are present here as well.

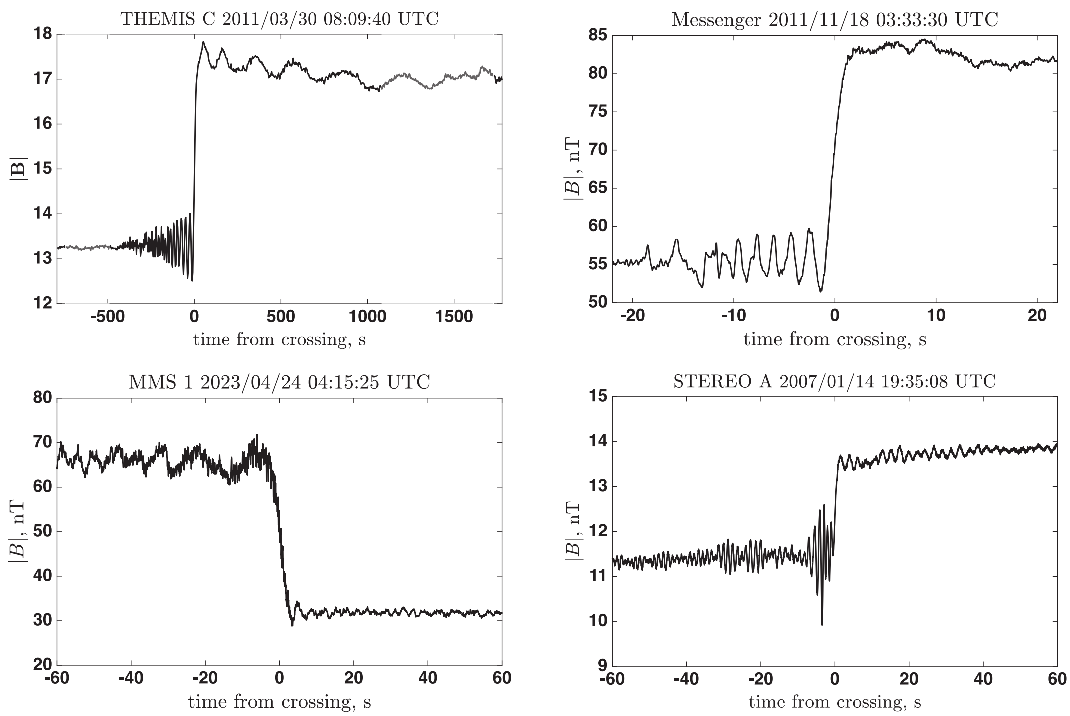

Figure 2. Four subcritical shocks. See details in the text.

The Mercury bow shock crossing by Messenger (top right) has $\theta_{Bn} \approx 70°$. There is a data gap in the plasma measurements, and the Mach number cannot be determined directly. However, the low magnetic compression $B_d/B_u \approx 1.47$ indicates $M_A < 2$. There is a standing precursor, while the overshoot is almost absent.

The bottom right panel shows an interplanetary shock with a very low magnetic compression of $B_d/B_u \approx 1.2$ and the Mach number of $M_a \approx 1.1$. The shock angle $\theta_{Bn} \approx 67°$. In the upstream region intermittent wavetrains are present, similar to the theoretically predicted time-dependent bursts (Granit & Gedalin, 2018).

The presence of an overshoot and downstream magnetic oscillations in very low-Mach-number shocks was earlier shown in observations at the Venusian bow shock (Balikhin et al., 2008). It has also been shown that subcritical quasi-parallel shocks do not differ quantitatively from quasi-perpendicular shocks (Balikhin et al., 2023).

The upstream part of the magnetic profile of a subcritical shock is well described within the two-fluid approach (Gedalin, 1998; Gedalin, Kushinsky, & Balikhin, 2015). The stationary one-dimensional equations in the approximation of quasineutrality and massless electrons read (Krall & Trivelpiece, 1973):

$$m_i v \partial_x \boldsymbol{v}_i = e\boldsymbol{E} + \frac{e}{c}\boldsymbol{v}_i \times \boldsymbol{B} - \hat{\boldsymbol{x}}\partial_x p_i - \nu(\boldsymbol{v}_i - \boldsymbol{v}_e) \tag{17}$$

$$0 = -e\boldsymbol{E} - \frac{e}{c}\boldsymbol{v}_e \times \boldsymbol{B} - \hat{\boldsymbol{x}}\partial_x p_e - \nu(\boldsymbol{v}_e - \boldsymbol{v}_i) \tag{18}$$

$$\hat{\boldsymbol{x}} \times \partial_x \boldsymbol{B} = \frac{4\pi}{c} ne(\boldsymbol{v}_i - \boldsymbol{v}_e), \tag{19}$$

$$nv = J = \text{const}, \quad \boldsymbol{E}_\perp = \text{const}, \quad B_x = \text{const} \tag{20}$$

Note that dissipation is necessary for the damping of the upstream precursor. In the above equations ν describes the friction between ions and electrons. This friction results in the resistivity $\eta = \nu/n_u e^2$. The wavelength and the damping length of the whistler precursor are determined by the dispersive and dissipative lengths

$$l_w = \frac{c \cos\theta_{Bn}}{M_A \omega_{pi}}, \quad l_d = \frac{c^2 \eta}{4\pi V_u} \tag{21}$$

The profiles predicted by the above equations are shown in Figure 3. The two-fluid approach cannot properly describe the ramp and downstream since ion kinetics plays an important role there. Yet, the two-fluid theory does provide an estimate of the ramp width in low-Mach number shocks with insignificant ion reflection, as well as the relation between the main magnetic field B_z and the noncoplanar magnetic field B_y.

To summarize, the upstream whistler precursor is the common feature of subcritical shocks, although the amplitudes vary from comparable to the main magnetic field jump to barely noticeable (Wilson et al., 2017). The upstream region of subcritical shocks is not contaminated by reflected ions, and therefore, the theoretical dispersive-dissipative two-fluid approach is appropriate. While the whistler dispersion is natural in a collisionless plasma, the mechanism of dissipation is not clear at present. The ramp width is typically of the order of the upstream ion convective gyroradius V_u/Ω_u, $\Omega_u = eB_u/m_p c$, or smaller. The magnetic moment conservation is not consistent with the entropy generation inside the shock transition (Gedalin, 2020a), which means that ion motion inside the shock transition is essentially non-adiabatic. This behavior precludes efficient usage of fluid approaches since the relation between the moments of the distribution function is unknown, unless we are able to solve the non-integrable equations of motion in the one-dimensional stationary fields of the shock front.

3.3. Quasi-Perpendicular Supercritical Shock

In supercritical shocks, reflected ions play an important role. The magnetic profiles of these shocks are more structured and complicated. From the observations of the terrestrial quasi-perpendicular bow shock, a "typical" shock profile was proposed (Scudder et al., 1986), shown schematically in Figure 4. The shock structure includes: (a) the wide foot ahead of the main transition, of the order of $0.5(V_u/\Omega_u)$ (Balikhin & Gedalin, 2022; Gosling & Thomsen, 1985; Leroy et al., 1982; Paschmann et al., 1982; Woods, 1969, 1971), (b) the ramp, at which the main magnetic field jump occurs, with the width $<c/\omega_{pi}$ (Hobara et al., 2010; Newbury et al., 1997, 1998), (c) the

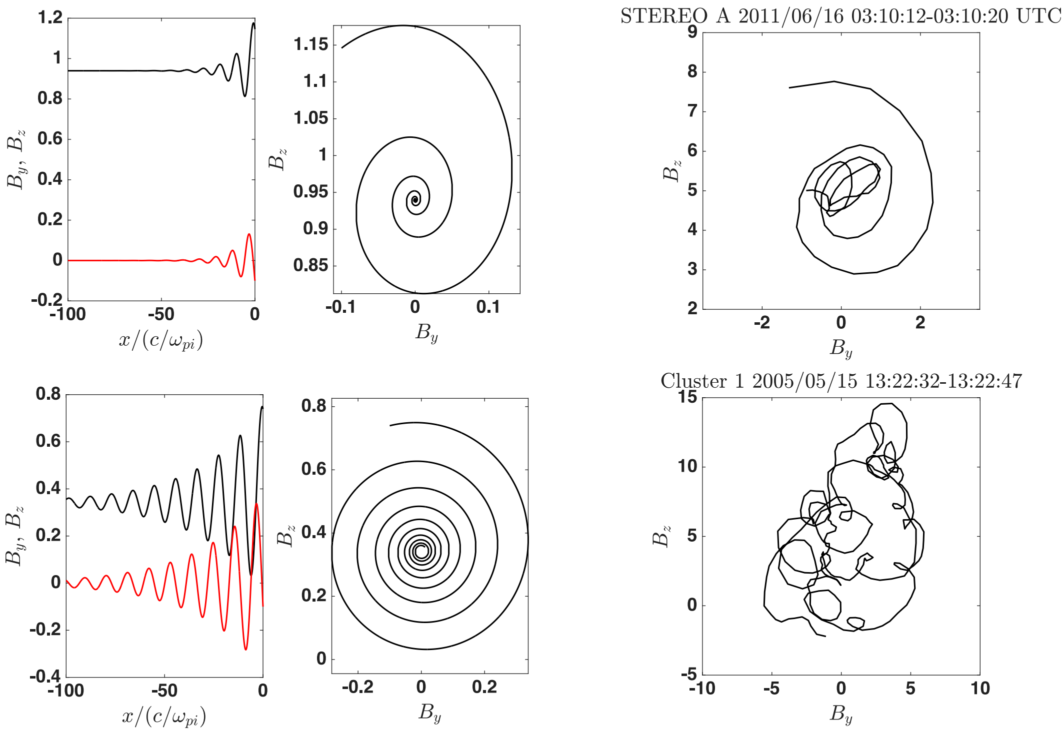

Figure 3. (Top row) $\theta_{Bn} = 70°$. (Bottom row) $\theta_{Bn} = 20°$. (Left column) The two tangential components as functions of position. (Middle column) The predicted hodogram of the tangential magnetic field. (Right column) The hodograms of two observed shocks, the top one is quasiperpendicular and the bottom one is quasiparallel.

overshoot, following the ramp, where the magnetic field exceeds the asymptotic downstream value (Livesey et al., 1982; Masters et al., 2013; Mellott & Livesey, 1987; Russell, Hoppe, & Livesey, 1982; Tatrallyay et al., 1984, 1997), and (d) the undershoot, following the overshoot, where the magnetic field is below the asymptotic downstream value. The undershoot may be followed by further magnetic oscillations (Sagdeev, 1966). The foot is explained as the increase of the magnetic field due to the current of the reflected-gyrating ions. The overshoot was also thought to be due to the reflected ions until is was shown that overshoots are present in subcritical shocks too (Balikhin et al., 2008). The downstream magnetic oscillations, including the overshoot, were found to be due to the kinematic collisionless relaxation (Balikhin et al., 2008; Gedalin, 2015, 2019b, 2019c; Gedalin, Friedman, & Balikhin, 2015; Ofman et al., 2009; Pope, 2020; Pope et al., 2019).

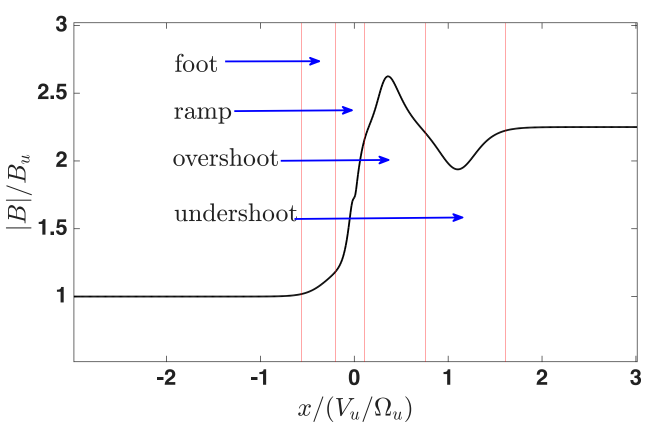

Figure 4. A sketch of the structured magnetic profile of a "typical" supercritical quasi-perpendicular shock. The approximate boundaries of the indicated regions are marked by vertical lines.

The shock used to derive the "typical" structure had $M_A = 7.7$ and was claimed to be nearly planar and stationary. The "typical" profile is relevant to the Earth bow shock with the Mach numbers typically in the range $5 < M_A < 10$, and is only a schematic representation of the features commonly observed in supercritical quasi-perpendicular shocks. The range of Mach numbers at supercritical heliospheric shocks is much larger, $2 \lesssim M_A \lesssim 75$ (Neugebauer, 2013; Neugebauer & Giacalone, 2005; Sulaiman et al., 2015, 2016). The magnetic structure may be quite complicated even at low Mach numbers, $M_A \sim 3$. Figure 5 shows two supercritical shocks with similar Mach numbers and angles. There is no foot as a monotonic increase of the magnetic field ahead of the ramp. Instead, there is a kind of precursor consisting of large-amplitude oscillations of the magnetic field, with some gradual increase of the average field. The precursor, the ramp, the overshoot, and the downstream magnetic oscillations are the common features of supercritical shocks.

A shock, for example, a planetary bow shock, is formed between two regions with different boundary conditions. Specifically, the asymptotic magnetic

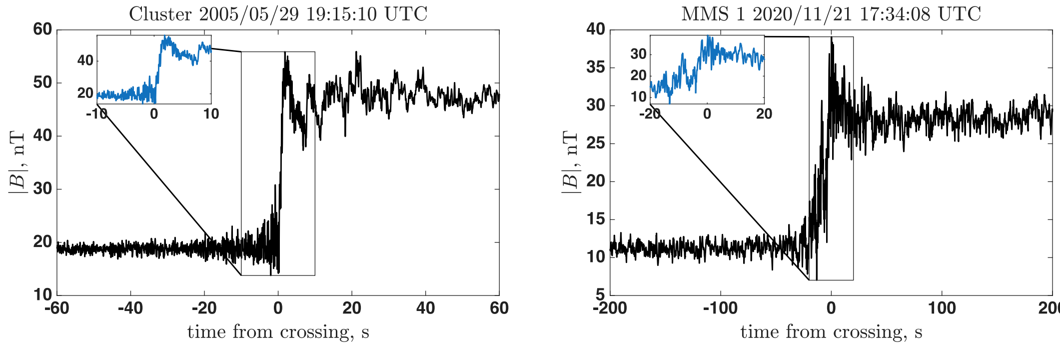

Figure 5. (Left panel) $M_A \approx 3.1$, $\theta_{Bn} \approx 69°$. (Right panel) $M_A \approx 3.2$, $\theta_{Bn} \approx 64°$.

fields on both sides are different. According to MHD, such a profile should steepen until it becomes a discontinuity. When the scale of a steepened ramp becomes smaller than the typical MHD scale, the dispersive effects (the whistler dispersion) come into play. The ramp generates a whistler ahead of it and does not steepen any longer (Krasnoselskikh et al., 2002, 2013; Lobzin et al., 2007). In this approach, the wavelength of the upstream phase-standing whistler should determine the width of the ramp. Such an estimate gives a correct qualitative dependence of the ramp width upon the Mach number and angle. However, it may be considered only as qualitative, as the ions become demagnetized inside the shock front, so that the standard dispersion relations are not valid anymore inside the shock transition. There is yet no quantitative theory explaining the ramp width and the adjacent precursor. The latter may be very different in different shocks, sometimes seemingly evolving into a series or sub-ramps.

The downstream oscillations are better understood. The theory of kinematic collisionless relaxation explains these oscillations in subcritical and supercritical shocks as well (Balikhin et al., 2008; Gedalin, 2019a, 2019b, 2019c; Gedalin, Friedman, & Balikhin, 2015; Ofman et al., 2009). The ion dynamics is discussed in Section 4.

Finally, non-planarity and time-dependence become progressively more important at higher Mach numbers. Analysis and interpretation of the shock profile features depend on the ability to represent the components of the fields in NIF. The first task is to determine the shock normal from the observations. Assuming one can reasonably identify the asymptotic, approximately uniform, upstream and downstream regions, the following mean values are calculated:

$$\boldsymbol{B} = \langle B\rangle, \quad n = \langle n\rangle, \quad \langle n\rangle, \quad \boldsymbol{V}^{(sp)} = \langle V\rangle \tag{22}$$

where $\langle\ldots\rangle$ in fact means averaging over time in the spacecraft frame, the averaging is done over the upstream and downstream regions (time intervals) separately, and superscript (sp) emphasizes the dependence of the velocity on the reference frame. The average quantities are used to determine the shock coordinates, (x, y, z) in our notation, from the coplanarity theorem (de Hoffmann & Teller, 1950; Schwartz, 1998). The magnetic coplanarity gives

$$\hat{z} = \frac{\Delta\boldsymbol{B}}{|\Delta\boldsymbol{B}|}, \qquad \boldsymbol{B} = \boldsymbol{B}_d - \boldsymbol{B}_u, \qquad \hat{m} = \frac{\boldsymbol{B}_u \times \Delta\boldsymbol{B}}{|\boldsymbol{B}_u \times \Delta\boldsymbol{B}|} \tag{23}$$

$$\hat{n} = \hat{m} \times \hat{z}, \qquad \hat{x} = \hat{n}\,\mathrm{sign}\left(\boldsymbol{V}_u^{(sp)} \cdot \hat{n}\right), \qquad \hat{y} = \hat{z} \times \hat{x} \tag{24}$$

The mixed coplanarity gives

$$\hat{z} = \frac{\Delta\boldsymbol{B}}{|\Delta\boldsymbol{B}|}, \qquad \hat{y} = \frac{\Delta\boldsymbol{V} \times \Delta\boldsymbol{B}}{|\Delta\boldsymbol{V} \times \Delta\boldsymbol{B}|}, \qquad \hat{x} = \hat{y} \times \hat{z}, \quad \Delta\boldsymbol{V} = \boldsymbol{V}_d^{(sp)} - \boldsymbol{V}_u^{(sp)} \tag{25}$$

The shock angle is then obtained from

$$\cos\theta_{Bn} = \frac{\hat{x} \cdot \boldsymbol{B}_u}{|\boldsymbol{B}_u|} \tag{26}$$

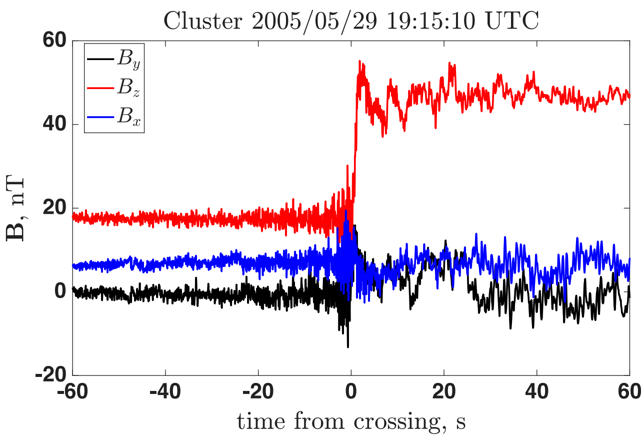

Figure 6. Three components of the supercritical shock, shown in Figure 5, left panel.

The mixed coplanarity Equation 25 requires reliable measurements of the velocity. Both ion and electron measured velocities may be used and may give different results, depending on the quality of measurements. Yet another method is to use the model normal for planetary shocks (see, e.g., Farris & Russell, 1994). The determination of the shock speed V_{sh} and the Mach number requires reliable measurements of the density:

$$V_{sh} = \left| \frac{\hat{x} \cdot \left(n_d \boldsymbol{V}_d^{(sp)} - n_u \boldsymbol{V}_u^{(sp)} \right)}{n_d - n_u} \right| \tag{27}$$

$$V_u = \frac{\hat{x} \cdot \left(\boldsymbol{V}_u^{(sp)} - \boldsymbol{V}_d^{(sp)} \right)}{1 - n_u/n_d} \tag{28}$$

$$v_A = \frac{B_u}{\sqrt{4\pi n_u m_p}}, \quad M_A = \frac{V_u}{v_A} \tag{29}$$

where ion or electron characteristics may be used. Ideally, the asymptotic densities and velocities of both species should be equal. Often, the cold solar wind is not well caught by the spacecraft equipment. Nevertheless, for subcritical shocks, usually the determination is good enough to accept the parameters as a viable approximation. In particular, the magnetic coplanarity is successful in most cases. For supercritical shocks, the proper identification of the upstream and downstream regions becomes more difficult because of the large magnetic oscillations. The mixed coplanarity normal and the model normal were shown to be in better agreement than all other methods (Gedalin et al., 2022), therefore, it is common to use the model shock normal for the shock angle determination.

Deviations from planarity become progressively stronger with the increase of the Mach number. Figure 6 presents the three components of the supercritical shock, shown in Figure 5, left panel. The magnetic coplanarity (24) was used. The normal component B_x, which is expected to be constant throughout the shock, if it were planar, strongly deviates from the upstream value inside the ramp. Variations of this component persist in the downstream region. These deviations from planarity are widely believed to be an indication of rippling (Gingell et al., 2017; Johlander et al., 2016, 2018; Lobzin et al., 2008; Lowe & Burgess, 2003; Moullard et al., 2006; Ofman & Gedalin, 2013). Rippling of quasi-perpendicular shocks is apparently related to the reflected ions gyrating in the foot. It was suggested that rippling develops in the foot due to an instability of these ions (Burgess & Scholer, 2007). Others claim rippling is a surface wave running in the overshoot (Johlander et al., 2018, 2023). It was also suggested that rippling is caused by amplification of non-local ion reflection (Gedalin, 2023a). An analytical model was proposed for rippling as a propagating surface wave localized in the ramp-overshoot region (Gedalin & Ganushkina, 2022) and further generalized to account for oblique propagation into the downstream region (Gedalin & Roytershteyn, 2024). Figure 7 illustrates a rippled shock for the model of a surface wave $\propto \cos(k_z z - \omega t)$ localized around the ramp. In this model, $\omega = 0.5\Omega_u$ and $\lambda = 2\pi/k_z = 4(V_u/\Omega_u)$. The amplitude of the rippling is $0.3D$, where $D = c/\omega_{pi}$ is the ramp width. The top left panel shows the 2D surface of $|B|$ in an arbitrary moment t. The bottom left panel illustrates the 2D pattern of the fields. The magnetic and electric fields are mutually consistent via the induction equation. The top right panel shows the magnetic field measured by the spacecraft moving across the shock with different v_x (measured in units of V_u) and $v_y = v_z = 0$. The bottom right panel shows the magnetic field measured by the spacecraft moving across the shock with different v_z and $v_x = 0.02V_u$, $v_y = 0$. In single spacecraft observations, it is easy to misinterpret the profile. Multi-spacecraft measurements with small spacecraft separations would show almost identical profiles. If these profiles look like the first three in Figure 7, bottom right, the most plausible interpretation is that a rippled shock is slowly crossed, especially if a sequence of similar loops and holes in the ion phase space in the downstream region is observed (Johlander et al., 2018). (see Figure 8).

Rippling means spatial inhomogeneity and time dependence in NIF. If ripples propagate at approximately constant speed along the shock front, as is usually assumed, then in the reference frame, moving with the ripples, the shock structure is essentially time independent. Another kind of temporal evolution of the shock profile is reformation, predicted by theory and numerical simulations (Galeev et al., 1988; Krasnoselskikh, 1985;

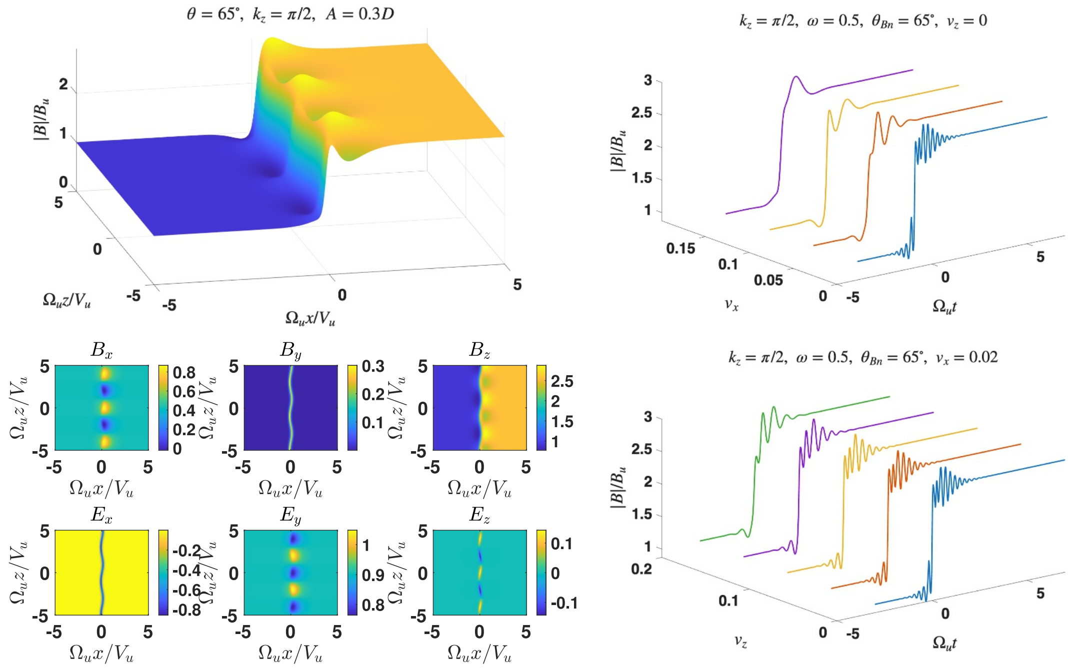

Figure 7. (Top left) The surface $|B|(x, z)$ of a rippled shock. (Bottom left) 2D patterns of $\boldsymbol{B}$ and $\boldsymbol{E}$. (Top right) $|B|(t)$ as measured by spacecraft crossing the shock with different v_x. (Bottom right) $|B|(t)$ as measured by spacecraft crossing the shock with different v_z.

Krasnoselskikh et al., 2002, 2013; Lembège & Savoini, 1992). In this regime, the ramp disappears and appears again, in a quasi-periodic or irregular manner, without a regular spatial pattern. Direct observations of the initial stages of steepening, leading to reformation, are rare (Dimmock et al., 2019). Most interpretations are indirect (Lefebvre et al., 2009; Liu et al., 2021; Lobzin et al., 2007; Mazelle et al., 2010; Tiu et al., 2011; Turner et al., 2021). Some of these interpretations refer to upstream structures detached from the main shock transition (Turner et al., 2021), so that the relation to the shock is questionable. Some other interpretations compare single-spacecraft measurements with 1D simulations (Tiu et al., 2011), suppressing rippling. The most convincing multi-spacecraft interpretations reveal the magnetic field behavior and ion reflection, corresponding to different stages of the profile steepening and relaxation after the shock front overturning (reformation) (Galeev et al., 1988; Krasnoselskikh, 1985; Krasnoselskikh et al., 2002), but it may be also explained by time-dependent rippling (Lefebvre et al., 2009; Liu et al., 2021; Lobzin et al., 2007; Mazelle et al., 2010), especially if ripples are not a monochromatic surface wave but a wavepacket of such waves.

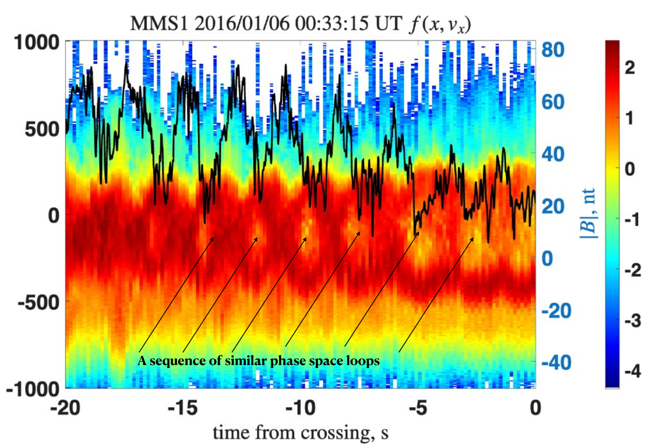

Figure 8. A sequence of similar loops and holes in the ion phase space in the downstream region.

To summarize, a quasi-perpendicular supercritical shock front has a narrow ramp, a large overshoot, downstream magnetic oscillations, a precursor, and often has a foot. The whole structure becomes non-planar and time-dependent at higher Mach numbers, typically as rippling. Reformation is also an option, although observationally, a strongly rippled shock can be misinterpreted as a reforming one.

3.4. Quasi-Parallel Supercritical Shocks

The accepted point of view at present is that quasi-parallel shocks differ qualitatively from quasi-perpendicular shocks. Figure 9 shows the magnetic field magnitude of a quasi-parallel, $\theta_{Bn} \approx 30^{\circ}$, shock.

In contrast with quasi-perpendicular shocks, no well-defined structure is clearly identified. The downstream magnetic field fluctuations look rather random. Such observations lead to the concept of a "patchwork" of large-

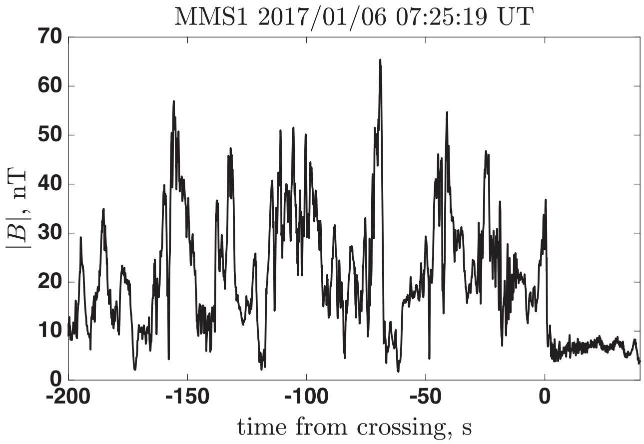

Figure 9. The magnetic field magnitude of a quasi-parallel, $\theta_{Bn} \approx 30°$, shock.

amplitude magnetic structures growing upstream of the shocks, drifting toward the shock, and converging there to form a shock transition and a downstream region lacking a structure (Burgess et al., 2005; Schwartz & Burgess, 1991). The distribution of the $\cos\theta_{Bn}$ of the observed terrestrial bow shock crossings is nearly uniform (see, e.g. Gedalin et al., 2021), with a drop for $\theta_{Bn} \approx 0$. The latter is because of the difficulties in identifying nearly parallel shocks. The structure of the quasi-parallel part of the Earth bow shock may be contaminated by large-amplitude upstream waves generated due to ions reflected from other parts of the shock. Interplanetary shocks are typically low-Mach-number supercritical shocks. Recently, observations in the vicinity of the Sun provided new information about how quasi-parallel shocks are built. Figure 10 shows the shock observed by Solar Orbiter on 30 October 2021 at 22:02:10 UT (Dimmock et al., 2023). The shock normal used in the plots was determined using magnetic coplanarity. The shock is not planar, but the variations of B_x are not shown here. The right column shows that the field inside the shock transition is well-structured, and the transition is sharp. A similar sharp transition at a quasi-parallel shocks was observed recently by the Parker Solar Probe (Jebaraj, Agapitov, Krasnoselskikh, et al., 2024). The shock front width was of on order of an ion inertial length, the shock became locally quasiperpendicular with a large overshoot in the transition region, and no upstream large-amplitude structures were observed, in contrast with the standard interpretation of a quasi-parallel shock as formed by merging of the upstream structures drifting toward the shock (Burgess & Scholer, 2013). A study of the structure of the MMS observed quasi-parallel shocks is currently underway. It was recently shown that in the downstream region of these shocks $\langle(\boldsymbol{B} - \langle\boldsymbol{B}\rangle)^2\rangle$ is comparable with $\langle\boldsymbol{B}\rangle^2$ and even can be much larger (Golan & Gedalin, 2025). Solar Orbiter and Parker Solar Probe measure shocks in an environment different from that of planetary bow shocks or interplanetary shocks at 1

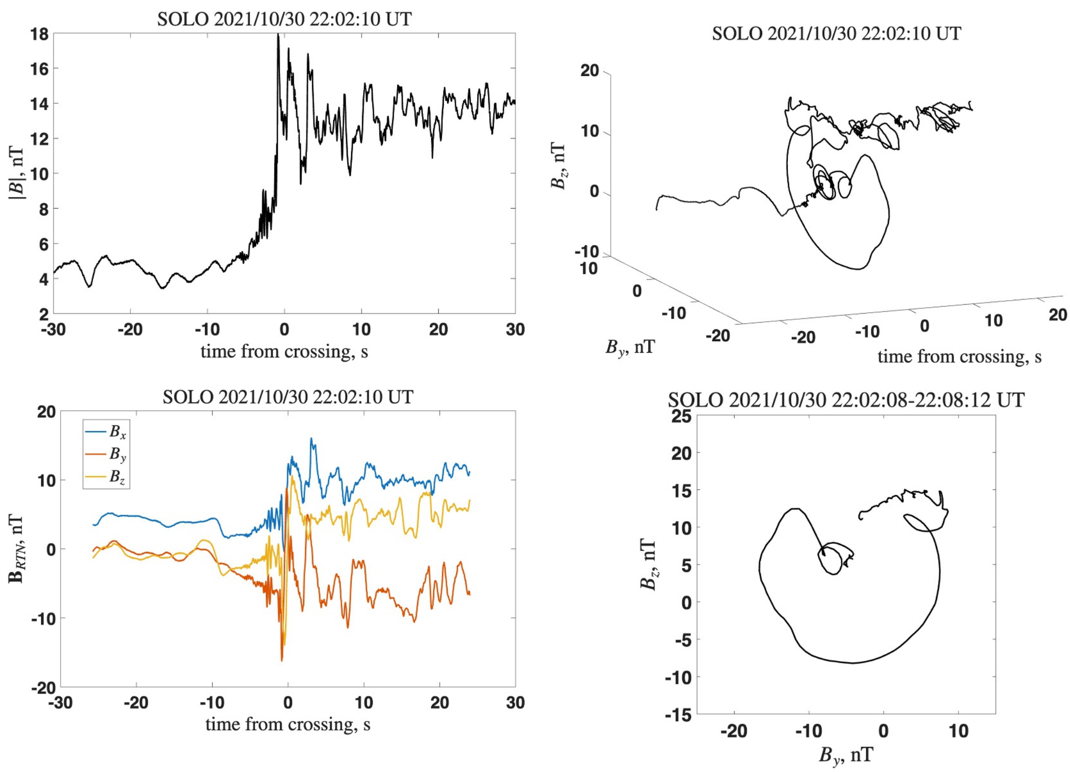

Figure 10. (Top left) The magnetic field magnitude. (Bottom left) Three magnetic field components in the spacecraft coordinates. (Top right) The tangential components (B_y, B_z) along the spacecraft trajectory. The normal was determined using magnetic coplanarity. (Bottom right) The hodogram of the tangential components in the shock transition.

AU. This allows us to test the theory developed mainly due to the observations at the Earth's bow shock, and understand what is common for various environments, and what modifications should be made to extend our current knowledge to a broader class of space plasma systems. In particular, in the near-Sun region, shocks produced by coronal mass ejections are observed near the site of their generation. One such shock has already been shown to accelerate particles up to the energies where electrons start to emit synchrotron radiation (Jebaraj, Agapitov, Gedalin, et al., 2024). So far, this is the only observation of shock-induced synchrotron emission in the heliosphere. Solar Orbiter shocks were observed at various heliocentric distances, which also gives information on the shock parameters evolution.

4. Plasma Processes at Shocks

4.1. Plasma Thermalization

Thermalization of species in a collisionless plasma is a result of the particle dynamics in the electromagnetic fields. The charged particle motion is affected by the macroscopic and microscopic fields inside the shock front. The macroscopic fields are the fields that were discussed in the previous section. These fields may be spatially inhomogeneous and/or time-dependent. The scales of the spatial inhomogeneity along the shock front can be as small as the electron inertial length c/ω_{pe} (Hobara et al., 2010; Newbury & Russell, 1996; Newbury et al., 1998). The rippling scales are larger (Gedalin & Ganushkina, 2022; Gingell et al., 2017; Johlander et al., 2016, 2018; Lobzin et al., 2008; Lowe & Burgess, 2003; Ofman & Gedalin, 2013; Omidi et al., 2021). The time-dependence of these fields is related to the propagating ripples, to reformation (Hellinger, 2002; Lefebvre et al., 2009; Lembège & Savoini, 1992; Liu et al., 2021; Lobzin et al., 2007; Mazelle et al., 2010; Tiu et al., 2011; Turner et al., 2021; Yuan et al., 2009), or to oscillations of the shock ramp, that may be an intrinsic feature of all shocks (Granit & Gedalin, 2018). Microscopic fields are those that have much smaller spatial and temporal scales, like the Debye-scale electric fields inside and around the ramp (Kamaletdinov et al., 2022, 2024; Vasko et al., 2018, 2020; Wang et al., 2020, 2021), or the short-wavelength whistler wavetrains (Wilson et al., 2017). In a collisionless plasma, the entropy phase-space density $-f\ln f$ does not change along the trajectory, since the Vlasov equation is equivalent to $df/dt = 0$ along the path. In a closed system, the exact entropy would be conserved. The problem of irreversibility in collisionless systems is well-known in relation to the Landau damping (Mouhot & Villani, 2011). In this case, the information is constantly transferred to smaller and smaller scales in the velocity space. While the exact entropy is conserved, the coarse-grained entropy increases. A shock is an open system. Thermalization, in the thermodynamic sense, should be accompanied by an increase in the entropy of the flow crossing the shock, as required by the Rankine-Hugoniot. Recently, an analysis of the electron entropy change across the shock front led to the conclusion that anomalous resistivity is insignificant (Agapitov et al., 2023). The major entropy increase was due to ions. It was suggested that gyrophase mixing may play the role of coarse-graining and that entropy increases when a proper averaging is performed (Gedalin, Friedman, & Balikhin, 2015). At present, there are no theoretical estimates of the coarse-grained entropy in shocks. Small-scale fluctuations may play the role of collisions in smoothing the fine-scale inhomogeneities in the velocity. The microphysics of irreversibility is still an open question.

4.2. Ion Heating

In a more general way, heating refers to the increase in the spread in the velocity space. This spread may not be isotropic and not even gyrotropic, that is $T_{ij} = p_{ij}/n$ (see Equation 12) is a tensor. The ion non-gyrotropy was observed at the Earth's bow shock (Li et al., 1995) and explained theoretically (Gedalin & Zilbersher, 1995) as a result of ion gyration starting at the shock crossing. Ions are not sensitive to small-scale fields (Gedalin, 2020b). Ion heating is illustrated in Figure 11. The ions are traced across the shock by solving the equations of motion.

$$\dot{\boldsymbol{v}} = \frac{q}{m}\left(\boldsymbol{E} + \frac{1}{c}\boldsymbol{v}\times\boldsymbol{B}\right) \tag{30}$$

in a model shock profile

$$B_z = B_u \sin\theta_{Bn}\left(\frac{R+1}{2} + \frac{R-1}{2}\tanh\frac{x}{D}\right) \tag{31}$$

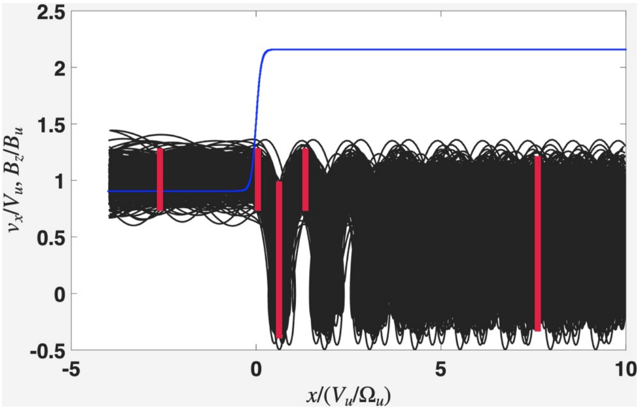

Figure 11. Velocities v_x of several ions crossing a shock front. The red lines roughly indicate the width of the distribution.

$$B_y = l_w \frac{dB_z}{dx}, \quad E_x = -k_E \frac{dB_z}{dx} \tag{32}$$

where l_w is given in Equation 21, $B_x = B_u \cos\theta_{Bn}$, $E_y = V_u B_u \sin\theta_{Bn}/c$, $E_z = 0$, and the coefficient k_E is determined from the cross-shock potential

$$-\int_{-\infty}^{\infty} eE_x dx = s\left(m_p V_u^2/2\right) \tag{33}$$

The Mach number M_A, the shock angle θ_{Bn}, the normalized cross-shock potential s, the magnetic compression of the main magnetic component R, and the ramp width D are variable parameters of the model. The equations of motion are solved in a normalized form. The cross-shock electric field of the model has a smooth profile, being a spatial averaging of the observed spiky field. We do not give the parameters for ion tracing in Figure 11 since it is for illustrative purposes only. It shows that each ion starts gyrating behind the ramp. Each ion has its own gyration speed and its own velocity along the downstream magnetic field, which causes gradual gyrophase mixing (Balikhin et al., 2008; Gedalin, 2015, 2020b; Gedalin, Friedman, & Balikhin, 2015; Ofman et al., 2009). The read strips roughly indicate the width of the distribution function in v_x at several positions. This width is the measure of the temperature at the position of a stripe. The larger the width, the higher the temperature. For each ion, entering the shock transition layer at $x = 0$ with the velocity (v_{0x}, v_{0y}, v_{0z}) and crossing it without stopping, the velocities $\left(v_{fx}, v_{fy}, v_{fz}\right)$ at the downstream edge of the ramp $x = D_r$ are (Gedalin, 1997).

$$v_{fx}^2 = v_{0x}^2 + \frac{2q}{m}\int_0^{D_r} E_x dx + \frac{2q}{mc}\int_0^{D_r} \left(v_y B_z - v_z B_x\right) dx \tag{34}$$

$$v_{fy} = \frac{q}{m}\int_0^{D_r} \left(\frac{E_y}{v_x} - \frac{B_z}{c}\right) dx \tag{35}$$

$$v_{fz} = \frac{q}{mc}\int_0^{D_r} \left(B_y - \frac{B_x v_z}{v_x}\right) dx \tag{36}$$

In general, the ion motion across the ramp is affected by both the electrostatic deceleration and magnetic deflection. The role of the magnetic deflection will be discussed later. For our present purposes, it is sufficient to consider the approximation $D_r \to 0$, keeping $\phi = -\int E_x dx$ finite. In this approximation, the velocity of the ion upon crossing the ramp, in the downstream fields $\boldsymbol{B}_d = B_u(\cos\theta_{Bn}, 0, R\sin\theta_{Bn})$, $\boldsymbol{E}_d = (0, V_u B_u \sin\theta_{Bn}/c, 0)$, is $\boldsymbol{v}_f = \left(\sqrt{v_{0x}^2 - 2e\phi/m_p}, v_{0y}, v_{0z}\right)$. The ion will drift with the speed $V_d \approx V_u(B_u/B_d)$, move along the magnetic field with the velocity $v_\parallel \approx v_{0z} + v_{fx}\cos\theta_{Bn}(B_u/B_d)$, and gyrate around the magnetic field with the speed $v_\perp \approx v_{fx} - V_d$. Both $v_\parallel$ and $v_\perp$ depend on the initial velocities, which means that different ions move along the magnetic field with different velocities and have different gyroradii. This dependence on the initial conditions causes gradual gyrophase mixing. The amount of the heating is determined by $v_\perp$, which is approximately given by $\sqrt{V_u^2 - 2e\phi/m_p} - V_d$. Thus, conversion of the energy of the directed flow into thermal energy occurs due to collisionless ion motion in the macroscopic fields of the shock front. If fluctuations are present, their role is in smoothing the distribution function, but the energy transfer is determined by the global magnetic field change and cross-shock potential. The latter reduces the heating of the directly transmitted ions. Heating due to wave-particle interaction is a multi-step process, which requires first exciting waves to reasonable amplitudes, thus taking energy from ions, and afterward returning a part of this energy to these ions. The efficiency of this process is low. Adiabatic heating due to the magnetic compression is incompatible with the entropy increase in shocks (Gedalin, 2020a). Figure 12 illustrates observations of the evolution of the reduced distribution function $f(x, v_x)$ across a shock where directly transmitted ions dominate ion heating. This shock is the same as in Figure 2, bottom left. The gyration of the whole ion distribution and collisionless relaxation are seen in the core.

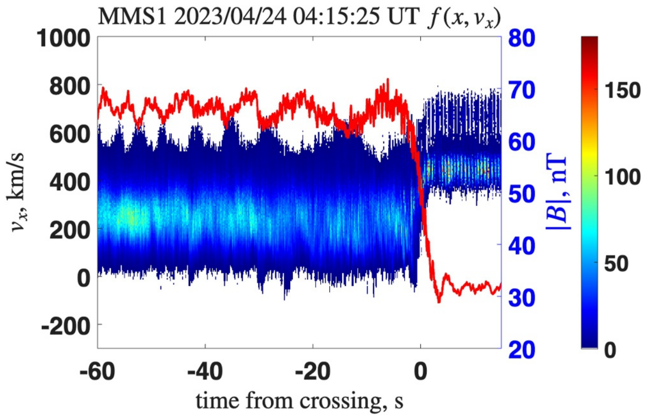

Figure 12. The reduced distribution function $f(x, v_x)$ across a shock where directly transmitted ions dominate ion heating.

4.3. Ion Reflection

In higher-Mach-number shocks, ion reflection becomes progressively more important. An ion is reflected if $v_x = 0$ somewhere behind the entry to the ramp, $x = 0$ in Equations 34–36, and the ion starts crossing the ramp again backwards. The reflection point may be inside the ramp or behind the ramp. The initial reflection model, the so-called specular reflection, suggested that ions are reflected by the cross-shock potential at the very entry to the ramp (Woods, 1969, 1971). Although numerous simulations and observations (Burgess et al., 1989; Gosling et al., 1982; Leroy, 1984; Leroy et al., 1982; Paschmann et al., 1981; Phillips & Robson, 1972; Sckopke et al., 1983, 1990) have clearly shown that ions penetrate the ramp and some even behind before being reflected, so that the magnetic deflection cannot be ignored, ion reflection is still erroneously referred to as "specular reflection," even though the estimate of the spatial size of the foot, based on this approach, is grossly incorrect (Balikhin & Gedalin, 2022; Gosling & Thomsen, 1985). Careful analyses of the ion motion in the macroscopic fields of the shock front have revealed the importance of the magnetic deflection and the two modes of the reflection: (a) the electrostatic mode, in which the effective cross-shock potential due to the electrostatic force and the magnetic force reverses the velocity of an ion inside the ramp, and (b) the magnetic mode, in which an ion crosses the ramp, gyrates behind the ramp, and comes back to the ramp due to the large gyration speed (Gedalin, 1996a, 2016; Sharma & Gedalin, 2023). For the electrostatic mode, higher cross-shock potentials are favorable. For the magnetic mode, lower cross-shock potentials are favorable. The fate of a reflected ion depends on the shock geometry and the initial velocity of the ion. In quasi-perpendicular shocks, $\theta_{Bn} \gtrsim 60°$, all or almost all ions moving backward inside the ramp eventually cross the shock toward downstream. If such an ion crosses the ramp completely and appears in the upstream region, it is a reflected-transmitted ion. If such an ion does not cross the ramp completely backward and reverses its motion toward downstream inside the ramp, it is a quasi-reflected ion. In oblique shocks, $\theta_{Bn} \lesssim 60°$, some reflected ions do not cross the shock toward downstream again but escape into the upstream region, constituting a distribution of backstreaming ions. In quasi-parallel shocks, $\theta_{Bn} \lesssim 30°$, all or almost all reflected ions are backstreaming ions, while the number of reflected-transmitted ions is small or even negligible. Though the mechanism of reflection is the same in quasi-perpendicular and quasi-parallel shocks, the effect of the reflected ions is quite different: in quasi-perpendicular shocks, they affect the downstream region, in quasi-parallel shocks, they affect the upstream region. In all cases, the initial velocities of the ions, which are reflected, are coming from the tail of the distribution of the incident ions, so that higher upstream v_T/V_u are favorable. In all cases, the reflected ions acquire superthermal energies during the reflection process, if viewed in NIF. The variety of ion trajectories is illustrated by Figure 13. Figure 14 illustrates ion reflection at quasi-perpendicular shocks. The shock is taken from the SHARP database (Ganushkina et al., 2024; Lalti, Khotyaintsev, Dimmock, et al., 2022) and has the parameters $M_A \approx 5$, $\theta_{Bn} \approx 70°$. The reflected-transmitted ions are present ahead of the ramp and cause deceleration of the flow. Behind the ramp, the gyroradii of the reflected-transmitted ions differ substantially from the gyroradii of the directly transmitted ions, so that their distribution exhibits different periodicity in the downstream region.

Figure 15 illustrates ion reflection at quasi-parallel shocks. The shock is also taken from the SHARP database and has the parameters $M_A \approx 8$, $\theta_{Bn} \approx 4°$. The reflected-backstreaming ions appear upstream in the form of bunches, indicating significant gyrating velocities. The downstream intermittency of the fields and the distribution may be due to the time dependence of the shock front.

The reflected-transmitted ions have gyration velocities $v_{r\perp} \sim (1.5-2)V_u$. These ions are superthermal. Even if their contribution to the downstream density n_{rd} is small, the contribution to the downstream temperature and kinetic pressure $\sim n_{rd} v_{r\perp}^2$ may be large and even dominant.

Figure 16 compares the ion distributions in the above-presented shocks, using slices in the $x - y$ plane. In the quasi-perpendicular shock, reflected-transmitted ions appear just ahead of the ramp. In the downstream region, both distributions of the transmitted ions (directly transmitted and reflected-transmitted) gyrate in a rather coherent way, and mixing occurs gradually. In the quasi-parallel shock, there appear reflected-backstreaming ions well ahead of the shock transition. The downstream distribution consists mainly of directly-transmitted ions and

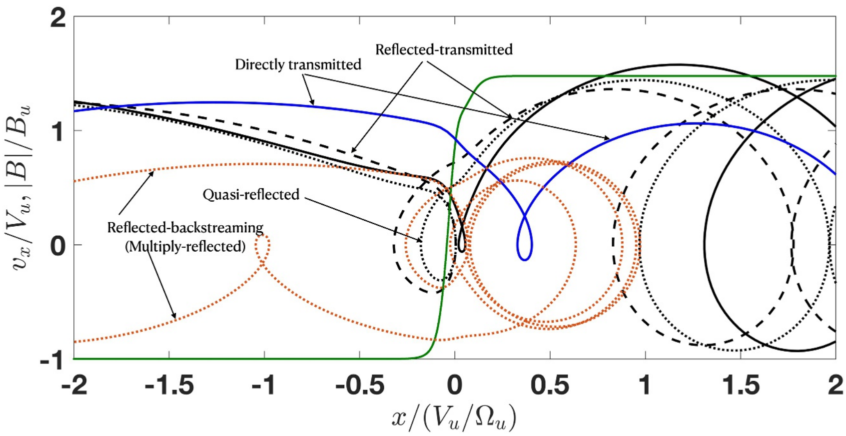

Figure 13. Some ion trajectories in a simplified model of an oblique shock front.

an irregular weak halo of superthermal ions, probably generated due to the time dependence of the shock front. Note that locally quasi-parallel shocks are quasi-perpendicular in the transition region.

At non-planar and time-dependent shocks, rippled or reforming, ion dynamics is similarly affected by the macroscopic fields, which are spatially and temporally inhomogeneous at the ion scales, namely, the ion inertial length or ion convective gyroradius and ion gyroperiod. The ion equations of motion are even farther from being integrable and treatable analytically, yet the basic processes are the same, only less regular. For example, ion reflection may become bursty, seen as bunches in Figure 17.

In summary, ion heating at the collisionless shock front occurs promptly due to the conversion of the directed flow energy into the energy of ion gyration. The process of conversion is non-local and may be spatially and temporally dependent. The role of small-scale fluctuations is further smoothing of the ion distribution function, which typically may have regions of low phase-space density, the so-called ion holes Johlander et al. (2016).

Various populations of backstreaming ions have been observed upstream of the Earth's bow shock, even at large distances from it: (a) field-aligned ion beams (Kucharek et al., 2004; Meziane, Wilber, Mazelle, LeQuéau, et al., 2004; Meziane, Wilber, Mazelle, Parks, & Hamza, 2004; Oka et al., 2005; Thomsen et al., 1983), (b) gyrophase-bunched ion beams (Mazelle, 2003; Meziane et al., 1997, 2001; Meziane, Wilber, Mazelle, LeQuéau, et al., 2004), and (c) diffuse ion population (Kis et al., 2004; Kucharek & Scholer, 1991; Moebius et al., 1987; Paschmann et al., 1981; Trattner et al., 2023). The latter contribute to the seed population of the shock accelerated ions (see, e.g., Trattner et al., 2023).

4.4. Electron Heating

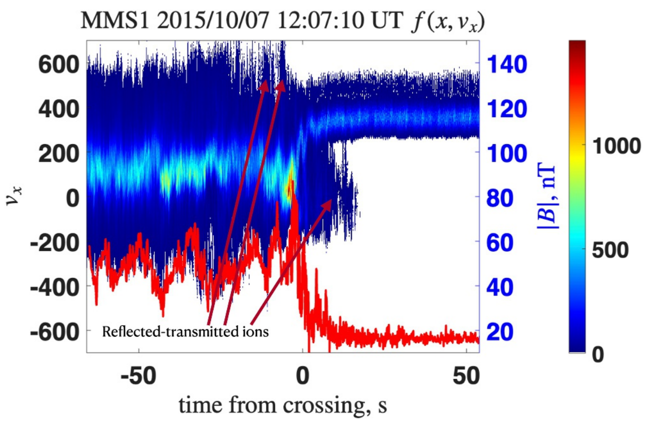

Figure 14. Reflected-transmitted ions in the foot and downstream of a quasi-perpendicular shock.

Electron heating is more sensitive to small-scale fields. Our view on electron heating in shocks evolved from the turbulent heating (Galeev, 1984) to the heating due to the laminar cross-shock potential and magnetic compression (Feldman et al., 1982; C. C. Goodrich & Scudder, 1984; Schwartz et al., 1987, 1988; Thomsen et al., 1985, 1987) to non-adiabatic heating of demagnetized electrons in the cross-shock potential (Balikhin & Gedalin, 1994; Balikhin et al., 1993) and back to the heating by turbulence which is not an ensemble of waves with random phases but a series of coherent small-scale electrostatic structures (Gedalin, 2020b, 2024; K. A. Goodrich et al., 2018; Kamaletdinov et al., 2022, 2024; Vasko et al., 2018, 2020; Wang et al., 2020). Electron heating occurs at the expense of the energy of the directed flow of incident ions. The main part of the difference between the energies of the incident and the decelerated downstream flows goes into ion heating. The rest is distributed among electron heating, particle acceleration, and magnetic field enhancement. Thus, the energy flow into electron heating is a multi-step process, which includes the generation of electrostatic fields as an

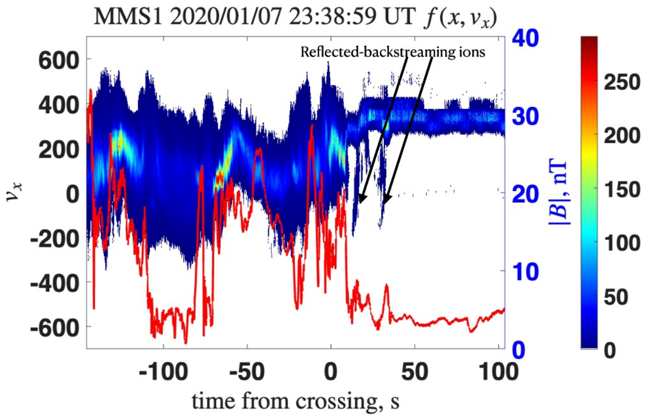

Figure 15. Reflected-backstreaming ions in the upstream of a quasi-parallel shock.

intermediate stage. It is expected that the overall cross-shock potential determines the amount of heating. The current view is that this potential is not due to a smooth macroscopic electrostatic field inside the shock front but is just an integrated $\phi = -\int E_x dx$, where E_x is built of many small-scale spikes, such that $-\int E_x dx$ across each spike is small, while the total $e\phi$ is a non-negligible part of $m_p V_u^2/2$. Derivation of the cross-shock potential from observations is a difficult task, and the errors are large, up to unphysical values (Dimmock et al., 2012). Observations of electron heating at supernova remnant (SNR) shocks hint at the dependence of the post-shock electron temperature on the Mach number as $T_e/\left(m_p V_u^2/2\right) \sim 1/M_A^2$ (Ghavamian et al., 2007, 2013; Rakowski et al., 2008; Raymond et al., 2023), although the errors are large and it is not excluded that there exists a lower limit on $T_e/\left(m_p V_u^2/2\right) \sim 1/M_A^2$, as suggested by a recent study at the Earth's bow shock (Gedalin et al., 2023). Since the distribution of the incident ion energy into channels other than ion heating is not well understood yet, a detailed explanation of the mechanism of the electron heating and of the available electron share is still a task in progress.

4.5. Particle Acceleration

A small number of ions and electrons are accelerated by shocks to energies far exceeding the thermal energies of the heated populations. The two major modes of shock acceleration are Shock Drift Acceleration (SDA) and DSA. In SDA (Webb et al., 1983), a charged particle remains in the vicinity of the shock front for a long time while drifting along the shock front in the direction of the motional electric field and thus acquiring energy. The primary challenge is to keep a particle trapped and prevent escaping upstream or proceeding downstream. The mechanism is efficient in quasi-perpendicular shocks. Variants of SDA include multiple reflection (Zank et al., 1996), surfing (Lee et al., 1996), meandering of the downstream magnetic field lines (Decker &

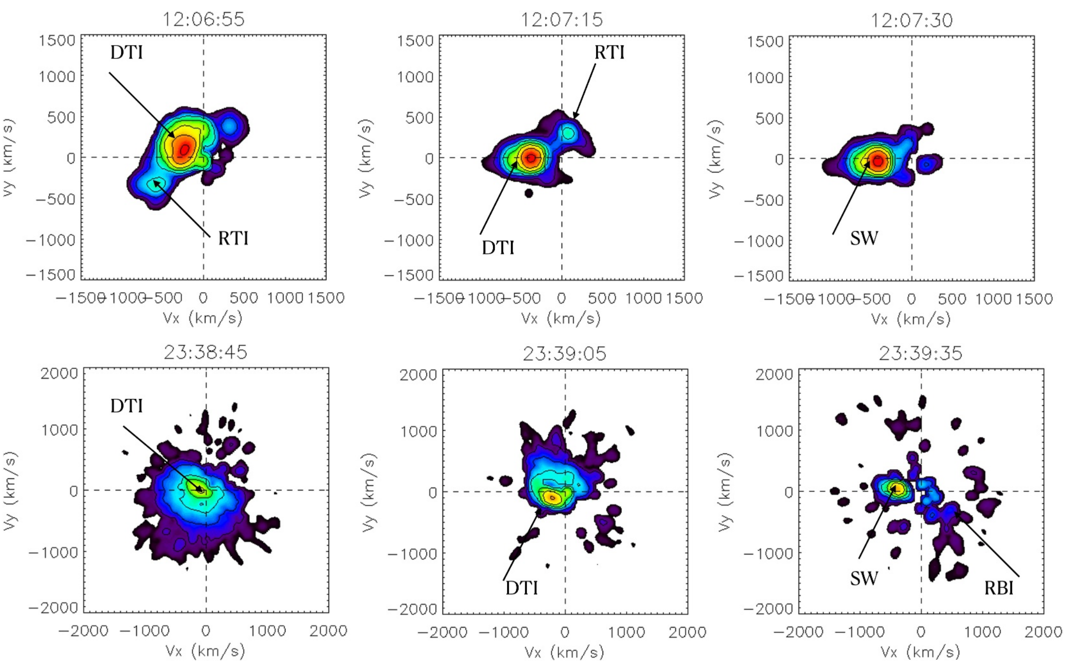

Figure 16. (Top row) Ion distributions in the quasi-perpendicular shock in Figure 14. (Bottom row) Ion distributions in the quasi-parallel shock in Figure 15. (Left column) The downstream region. (Middle column) The transition region. (Right column) The upstream region. Acronyms: DTI, directly transmitted ions; RTI, reflected-transmitted ions; RBI, reflected-backstreaming ions; SW, solar wind.

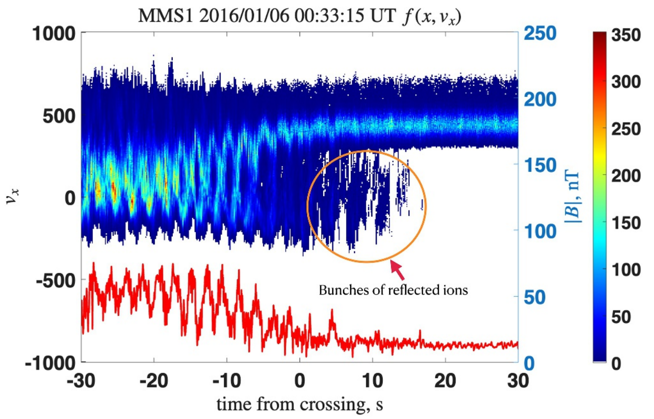

Figure 17. Ion dynamics and bursty reflection at a rippled quasi-perpendicular shock.

Vlahos, 1985), large-amplitude upstream fluctuations of the magnetic field (Giacalone & Jokipii, 2006), or additional turbulent scattering inside the shock front (Katou & Amano, 2019).

The prevailing view is that SDA is limited, and acceleration to high energies occurs within the DSA (Axford et al., 1977; Bell, 1978; Blandford & Eichler, 1987; Blandford & Ostriker, 1978; Drury, 1983; Krymskii, 1977; Toptyghin, 1980). In DSA, charged particles acquire energy due from the flow compression due to the shock transition by means of multiple front crossings and scattering on magnetic fluctuations in the upstream and downstream regions far from the shock transition (Jokipii, 1966a, 1966b; Skilling, 1975a, 1975b, 1975c). In the plasma flow frame, the particles, initially moving away from the shock, reverse their motion and are convected by the flow to cross the shock again and again. Energization occurs due to the difference between the upstream and downstream flow speeds. The role of the shock is to ensure these speeds are different and to establish the continuous matching of the upstream and downstream distributions at the shock transition. The slope of the spectrum $dN/dp = 4\pi p^2 f(p) \sim p^{-\alpha}$ is determined by this matching (Blandford & Eichler, 1987; Drury, 1983). Here p is the magnitude of the momentum and $f(p)$ is the isotropic part of the distribution function. The matching conditions depend on the shock parameters (Gedalin et al., 2016; Gedalin, Dröge, & Kartavykh, 2015), although this dependence is rarely taken into account. In the standard DSA, assuming continuity of the distribution function at the shock, the spectral index takes the simple form $\alpha = (r + 2)/(r - 1)$, where $r = N_d/N_u$ is the compression ratio. The maximum theoretical compression ratio for $M_A \to \infty$ is $r = 4$, which gives $\alpha = 2$. The maximum acceleration energy is determined by the time the particles are confined to the shock before escaping. Therefore, large-scale SNR shocks are more efficient accelerators than heliospheric shocks, also because of their higher velocities. Yet, recently, a near-Sun collisionless shock was observed having some properties resembling those of SNR shocks, including particle acceleration and synchrotron radiation from accelerated electrons (Jebaraj, Agapitov, Gedalin, et al., 2024; Jebaraj, Agapitov, Krasnoselskikh, et al., 2024). The scatterers (magnetic fluctuations) are widely believed to be produced or enhanced by the accelerated particles themselves (Bell, 2004). Within the heliosphere the propagation of high-energy particles and their acceleration at interplanetary shocks is often studied with the focused transport equation approach (see, e.g., Droege, 1994, and references therein). The effect of accelerated particles on the shock, in particular, the gradual magnetic field increase in a long precursor, is often studied within the approach of self-consistent modification (see, e.g., Malkov et al., 2010, and references therein).

In all cases, the mechanisms of acceleration are efficient for charged particles which already have sufficiently superthermal energy, which poses the problem of injection, that is, generation of a superthermal seed population directly from the incident thermal distributions (Malkov & Völk, 1998). The mechanism of injection is not well understood at present, although several suggestions have been tested in simulations. Understanding the acceleration of electrons is more difficult, since electrons have to be accelerated to much higher Lorentz factors to be able to be scattered by the same fluctuations that scatter ions. In the last years, pre-acceleration of electrons by whistlers has gained substantial attention (Shi, Artemyev, et al., 2023; Shi, Tonoian, et al., 2023).

A more detailed description of the shock acceleration mechanisms would require a separate review. It is beyond the scope of the present paper devoted to the structure of the shock transition region and the physical process inside it.

5. Implications for Astrophysical Shocks

At present, much more knowledge about the structure of shocks is collected on heliospheric shocks, at Alfvén Mach numbers $M_A < 100$, than it is possible to infer about strong SNR shocks with $M_A \gtrsim 100$ and possibly $M_A \sim 10^3$. Two extreme views exist about the possible extrapolation of the knowledge of heliospheric shocks onto SNR shocks. The pessimistic view claims that there are inevitable significant qualitative changes in physics when crossing some large, unknown today, Mach number. The optimistic view, adopted by us, suggests that the laws of physics do not change, and one has only to understand how to properly scale the parameters of, for example, heating and magnetic enhancement, with the Mach number. The optimistic point of view has gained support with the observations of a heliospheric shock similar in part to astrophysical shocks (Jebaraj, Agapitov, Gedalin, et al., 2024; Jebaraj, Agapitov, Krasnoselskikh, et al., 2024). Theory is yet to be adjusted to the new observations.

An interesting recent development, which may be directly relevant to astrophysical shocks, is the discovery of shocks with persistent large downstream magnetic oscillations (Golan & Gedalin, 2025). In these shocks the rms magnetic field $\sqrt{\langle \boldsymbol{B}^2 \rangle}$ may greatly exceed the mean magnetic field magnitude $|\langle \boldsymbol{B} \rangle|$. The latter is strongly limited by the standard Rankine-Hugoniot relations by $B_d/B_u \leq 4$. The presence of high non-evading pressure of magnetic fluctuations requires reconsideration of the boundary conditions at the shock front (Gedalin, 2023b, 2023c) and may have also immediate implications for the estimates of the magnetic field at SNR shocks and the mechanism of electromagnetic emission by accelerated electrons there (Greco et al., 2023).

6. Conclusions and Perspectives

A collisionless shock is a multiscale system formed and maintained by strongly interaction of charged particles and fields at all scales. This review is devoted to the ion scale, that is, the scale of the magnetic variations which are referred to as the shock structure, which is best understood, at this stage. Our theoretical understanding is mainly qualitative since the equations of motion are non-integrable, and there is no way to solve the Vlasov equations self-consistently. However, some of the features, like the ion heating or overshoot strength, may be quantitatively estimated. These estimates, at present, are largely based on the conservation laws in the nearly planar and time-independent approximation. The state-of-art high-resolution measurements by MMS are expected to provide clues for further development of the theory.

Conflict of Interest

The authors declare no conflicts of interest relevant to this study.

Availability Statement

All the data used in the review resides on publicly accessible servers. A number of shock databases are available. The SHARP shock database (Ganushkina et al., 2024; Lalti, Khotyaintsev, Graham, et al., 2022) is at https://sharp.fmi.fi/shock-database/. A list of Cluster shocks was compiled by Kruparova et al. (2019). A list of STEREO shocks is compiled and maintained by Lan Jian at https://stereo-ssc.nascom.nasa.gov/data/ins_data/impact/level3/. Wind, ACE, and DISCOVR shock lists are at https://lweb.cfa.harvard.edu/shocks/. A list of interplanetary shocks observed by Artemis (THEMIS A and B) is provided at https://themis.ssl.berkeley.edu/data/themis/events/. The THEMIS data can be found at https://themis.igpp.ucla.edu. The MMS data resides on https://lasp.colorado.edu/mms/sdc/public/. The Cluster data is at https://csa.esac.esa.int/csa-web/. The STEREO data can be accessed through https://stereo-ssc.nascom.nasa.gov/spaceweather.shtml. The Venus Express data can be accessed at https://www.cosmos.esa.int/web/psa/venus-express. The planetary bow shock (Mercury, Mars, Saturn) data can be accessed through https://pds-ppi.igpp.ucla.edu/index.jsp. The Parker Solar Probe shock list and data are at https://parker.gsfc.nasa.gov/shocks.html. For the Solar Orbiter data, see https://www.cosmos.esa.int/web/soar/getting-to-data. A database of Solar Orbiter shocks was recently released (Trotta et al., 2025), with a link https://data.serpentine-h2020.eu/catalogs/shock-sc25/. In most cases, the data can be obtained from https://cdaweb.gsfc.nasa.gov. In the preparation of the paper, IRFU-Matlab (https://github.com/irfu/irfu-matlab) and IDL Spedas (https://spedas.org) software were used.

Acknowledgments
All figures in the paper are prepared anew. The IRFU-MATLAB software was used in preparation of the plots of reduced distributions. The SPEDAS-IDL software was used in the preparation of slices. This paper is dedicated to the memory of Michael Balikhin, who passed away on 26 October 2025. Michael was our inspirational colleague and dear friend for more than 40 years.

References

Acuña, M. H., Curtis, D., Scheifele, J. L., Russell, C. T., Schroeder, P., Szabo, A., & Luhmann, J. G. (2008). The STEREO/IMPACT Magnetic Field Experiment. *Space Science Reviews*, *136*(1–4), 203–226. https://doi.org/10.1007/s11214-007-9259-2

Adlam, J. H., & Allen, J. E. (1958). The structure of strong collision-free hydromagnetic waves. *The Philosophical Magazine: A Journal of Theoretical Experimental and Applied Physics*, *3*(29), 448–455. https://doi.org/10.1080/14786435808244566

Agapitov, O. V., Krasnoselskikh, V., Balikhin, M., Bonnell, J. W., Mozer, F. S., & Avanov, L. (2023). Energy repartition and entropy generation across the Earth's bow shock: MMS Observations. *The Astrophysical Journal*, *952*(2), 154. https://doi.org/10.3847/1538-4357/acdb7b

Auster, H. U., Glassmeier, K. H., Magnes, W., Aydogar, O., Baumjohann, W., Constantinescu, D., et al. (2008). The THEMIS fluxgate magnetometer. *Space Science Reviews*, *141*(1–4), 235–264. https://doi.org/10.1007/s11214-008-9365-9

Axford, W. I. (1962). The interaction between the solar wind and the Earth's magnetosphere. *Journal of Geophysical Research*, *67*(10), 3791–3796. https://doi.org/10.1029/JZ067i010p03791

Axford, W. I., Leer, E., & Skadron, G. (1977). The acceleration of cosmic rays by shock waves. *International Cosmic Ray Conference*, *11*, 132–137.
Bale, S. D., Goetz, K., Harvey, P. R., Turin, P., Bonnell, J. W., Dudok de Wit, T., et al. (2016). The FIELDS Instrument Suite for Solar Probe Plus. *Space Science Reviews*, *204*(1–4), 49–82. https://doi.org/10.1007/s11214-016-0244-5
Balikhin, M., & Gedalin, M. (1994). Kinematic mechanism of electron heating in shocks: Theory vs observations. *Geophysical Research Letters*, *21*(9), 841–844. https://doi.org/10.1029/94GL00371
Balikhin, M., & Gedalin, M. (2022). Collisionless shocks in the heliosphere: Foot width revisited. *The Astrophysical Journal*, *925*(1), 90. https://doi.org/10.3847/1538-4357/ac3bb3
Balikhin, M., Gedalin, M., & Petrukovich, A. (1993). New mechanism for electron heating in shocks. *Physical Review Letters*, *70*(9), 1259–1262. https://doi.org/10.1103/PhysRevLett.70.1259
Balikhin, M. A., Gedalin, M., Walker, S. N., Agapitov, O. V., & Zhang, T. (2023). Structure of a Quasi-parallel shock front. *The Astrophysical Journal*, *959*(2), 130. https://doi.org/10.3847/1538-4357/ad0b71
Balikhin, M. A., Zhang, T. L., Gedalin, M., Ganushkina, N. Y., & Pope, S. A. (2008). Venus Express observes a new type of shock with pure kinematic relaxation. *Geophysical Research Letters*, *35*(1), L01103. https://doi.org/10.1029/2007GL032495
Balogh, A., Carr, C. M., Acuña, M. H., Dunlop, M. W., Beek, T. J., Brown, P., et al. (2001). The Cluster Magnetic Field Investigation: Overview of in-flight performance and initial results. *Annales Geophysicae*, *19*(10/12), 1207–1217. https://doi.org/10.5194/angeo-19-1207-2001
Bell, A. R. (1978). The acceleration of cosmic rays in shock fronts. I. *Monthly Notices of the Royal Astronomical Society*, *182*(2), 147–156. https://doi.org/10.1093/mnras/182.2.147
Bell, A. R. (2004). Turbulent amplification of magnetic field and diffusive shock acceleration of cosmic rays. *Monthly Notices of the Royal Astronomical Society*, *353*(2), 550–558. https://doi.org/10.1111/j.1365-2966.2004.08097.x
Blandford, R., & Eichler, D. (1987). Particle acceleration at astrophysical shocks: A theory of cosmic ray origin. *Physics Reports*, *154*(1), 1–75. https://doi.org/10.1016/0370-1573(87)90134-7
Blandford, R. D., & Ostriker, J. P. (1978). Particle acceleration by astrophysical shocks. *The Astrophysical Journal Letters*, *221*, L29–L32. https://doi.org/10.1086/182658
Bonnell, J. W., Mozer, F. S., Delory, G. T., Hull, A. J., Ergun, R. E., Cully, C. M., et al. (2008). The Electric Field Instrument (EFI) for THEMIS. *Space Science Reviews*, *141*(1–4), 303–341. https://doi.org/10.1007/s11214-008-9469-2
Burgess, D., Lucek, E. A., Scholer, M., Bale, S. D., Balikhin, M. A., Balogh, A., et al. (2005). Quasi-parallel shock structure and processes. *Space Science Reviews*, *118*(1), 205–222. https://doi.org/10.1007/s11214-005-3832-3
Burgess, D., & Scholer, M. (2007). Shock front instability associated with reflected ions at the perpendicular shock. *Physics of Plasmas*, *14*(1), 012108. https://doi.org/10.1063/1.2435317
Burgess, D., & Scholer, M. (2013). Microphysics of quasi-parallel shocks in collisionless plasmas. *Space Science Reviews*, *178*(2–4), 513–533. https://doi.org/10.1007/s11214-013-9969-6
Burgess, D., Wilkinson, W. P., & Schwartz, S. J. (1989). Ion distributions and thermalization at perpendicular and quasi-perpendicular supercritical collisionless shocks. *Journal of Geophysical Research*, *94*(A7), 8783–8792. https://doi.org/10.1029/JA094iA07p08783
Coroniti, F. V. (1970). Dissipation discontinuities in hydromagnetic shock waves. *Journal of Plasma Physics*, *4*(2), 265–282. https://doi.org/10.1017/s0022377800004992
Davis, L., Lust, R., & Schlüter, A. (1958). The structure of hydromagnetic shock waves: I. Non linear hydromagnetic waves in a cold plasma. *Zeitschrift für Naturforschung A*, *13*(11), 916–936. https://doi.org/10.1515/zna-1958-1102
Decker, R. B., & Vlahos, L. (1985). Shock drift acceleration in the presence of waves. *Journal of Geophysical Research*, *90*(A1), 47–56. https://doi.org/10.1029/JA090iA01p00047
de Gasperin, F., Rudnick, L., Finoguenov, A., Wittor, D., Akamatsu, H., Brüggen, M., et al. (2022). MeerKAT view of the diffuse radio sources in Abell 3667 and their interactions with the thermal plasma. *Astronomy & Astrophysics*, *659*, A146. https://doi.org/10.1051/0004-6361/202142658
de Hoffmann, F., & Teller, E. (1950). Magneto-hydrodynamic shocks. *Physical Review*, *80*(4), 692–703. https://doi.org/10.1103/PhysRev.80.692
Dimmock, A. P., Balikhin, M. A., Krasnoselskikh, V. V., Walker, S. N., Bale, S. D., & Hobara, Y. (2012). A statistical study of the cross-shock electric potential at low Mach number, quasi-perpendicular bow shock crossings using Cluster data. *Journal of Geophysical Research*, *117*(A2), 02210. https://doi.org/10.1029/2011JA017089
Dimmock, A. P., Gedalin, M., Lalti, A., Trotta, D., Khotyaintsev, Y. V., Graham, D. B., et al. (2023). Backstreaming ions at a high Mach number interplanetary shock - Solar Orbiter measurements during the nominal mission phase. *Astronomy & Astrophysics*, *679*, A106. https://doi.org/10.1051/0004-6361/202347006
Dimmock, A. P., Russell, C. T., Sagdeev, R. Z., Krasnoselskikh, V., Walker, S. N., Carr, C., et al. (2019). Direct evidence of nonstationary collisionless shocks in space plasmas. *Science Advances*, *5*(2), eaau9926. https://doi.org/10.1126/sciadv.aau9926
Droege, W. (1994). Transport of solar energetic particles. *Astrophysical Journal Supplement*, *90*, 567–576. https://doi.org/10.1086/191876
Drury, L. O. (1983). An introduction to the theory of diffusive shock acceleration of energetic particles in tenuous plasmas. *Reports on Progress in Physics*, *46*(8), 973–1027. https://doi.org/10.1088/0034-4885/46/8/002
Ergun, R. E., Tucker, S., Westfall, J., Goodrich, K. A., Malaspina, D. M., Summers, D., et al. (2016). The axial double probe and fields signal processing for the MMS mission. *Space Science Reviews*, *199*(1–4), 167–188. https://doi.org/10.1007/s11214-014-0115-x
Farris, M. H., & Russell, C. T. (1994). Determining the standoff distance of the bow shock: Mach number dependence and use of models. *Journal of Geophysical Research*, *99*(A9), 17681–17689. https://doi.org/10.1029/94JA01020
Farris, M. H., Russell, C. T., & Thomsen, M. F. (1993). Magnetic structure of the low beta, quasi-perpendicular shock. *Journal of Geophysical Research*, *98*(A9), 15285–15294. https://doi.org/10.1029/93JA00958
Feldman, W., Bame, S., Gary, S., Gosling, J., McComas, D., Thomsen, M., et al. (1982). Electron heating within the Earth's bow shock. *Physical Review Letters*, *49*(3), 199–201. https://doi.org/10.1103/PhysRevLett.49.199
Fishman, F., Kantrowitz, A., & Petschek, H. (1960). Magnetohydrodynamic shock wave in a collision-free plasma. *Reviews of Modern Physics*, *32*(4), 959–966. https://doi.org/10.1103/RevModPhys.32.959
Formisano, V., Russell, C. T., Means, J. D., Greenstadt, E. W., Scarf, F. L., & Neugebauter, M. (1975). Collisionless shock waves in space - A very high beta structure. *Journal of Geophysical Research*, *80*(16), 2013–2022. https://doi.org/10.1029/JA080i016p02013
Galeev, A. A. (1984). The heating and acceleration of electrons by shocks. *Advances in Space Research*, *4*(2–3), 255–263. https://doi.org/10.1016/0273-1177(84)90319-3
Galeev, A. A., Krasnoselskikh, V. V., & Lobzin, V. V. (1988). Fine structure of the front of a quasi-perpendicular supercritical collisionless shock wave. *Fizika Plazmy*, *14*, 1192–1200.

Galvin, A. B., Kistler, L. M., Popecki, M. A., Farrugia, C. J., Simunac, K. D. C., Ellis, L., et al. (2008). The Plasma and Suprathermal Ion Composition (PLASTIC) Investigation on the STEREO Observatories. *Space Science Reviews*, *136*(1–4), 437–486. https://doi.org/10.1007/s11214-007-9296-x

Ganushkina, N. Y., van de Kamp, M., Hoppe, T., Dubyagin, S., Gedalin, M., Dimmock, A., et al. (2024). SHARP shock database. *Journal of Geophysical Research: Space Physics*, *129*(7), e2024JA032625. https://doi.org/10.1029/2024JA032625

Gardner, C., Goertzel, H., Grad, H., Morawetz, C., Rose, M., & Rubin, H. (1958). Hydromagnetic shock waves in high-temperature plasmas. In *Proceedings of the 2nd U. N. International Conference on the Peaceful Uses of Atomic Energy* (Vol. 31, p. 230). United Nations.

Gedalin, M. (1996a). Ion reflection at the shock front revisited. *Journal of Geophysical Research*, *101*(A), 4871–4878. https://doi.org/10.1029/95JA03669

Gedalin, M. (1996b). Transmitted ions and ion heating in nearly perpendicular low-Mach number shocks. *Journal of Geophysical Research*, *101*(A), 15569–15578. https://doi.org/10.1029/96JA00924

Gedalin, M. (1997). Ion heating in oblique low-Mach number shocks. *Geophysical Research Letters*, *24*(2), 2511–2514. https://doi.org/10.1029/97GL02524

Gedalin, M. (1998). Low-frequency nonlinear stationary waves and fast shocks: Hydrodynamical description. *Physics of Plasmas*, *5*(1), 127–132. https://doi.org/10.1063/1.872681

Gedalin, M. (2015). Collisionless relaxation of non-gyrotropic downstream ion distributions: Dependence on shock parameters. *Journal of Plasma Physics*, *81*(6), 905810603. https://doi.org/10.1017/S0022377815001154

Gedalin, M. (2016). Transmitted, reflected, quasi-reflected, and multiply reflected ions in low-Mach number shocks. *Journal of Geophysical Research: Space Physics*, *121*(1), 10. https://doi.org/10.1002/2016JA023395

Gedalin, M. (2019a). How non-stationary are moderately supercritical shocks? *Journal of Plasma Physics*, *85*(5), 905850505. https://doi.org/10.1017/S0022377819000692

Gedalin, M. (2019b). Kinematic collisionless relaxation and time dependence of supercritical shocks with alpha particles. *The Astrophysical Journal*, *880*(2), 140. https://doi.org/10.3847/1538-4357/ab2bee

Gedalin, M. (2019c). Kinematic collisionless relaxation of ions in supercritical shocks. *Frontiers in Physics*, *7*, 692. https://doi.org/10.3389/fphy.2019.00114

Gedalin, M. (2020a). Inconsistency of magnetic-moment conservation with entropy increase in collisionless shocks. *Physical Review E - Statistical Physics, Plasmas, Fluids, and Related Interdisciplinary Topics*, *102*(1), 1–4. https://doi.org/10.1103/PhysRevE.102.013201

Gedalin, M. (2020b). Large-scale versus small-scale fields in the shock front: Effect on the particle motion. *The Astrophysical Journal*, *895*(1), 59. https://doi.org/10.3847/1538-4357/ab8af0

Gedalin, M. (2023a). Non-locality of ion reflection at the shock front: Dependence on the shock angle. *Journal of Plasma Physics*, *89*(4), 905890416. https://doi.org/10.1017/S0022377823000831

Gedalin, M. (2023b). Rankine–Hugoniot relations and magnetic field enhancement in turbulent shocks. *The Astrophysical Journal*, *958*(1), 2. https://doi.org/10.3847/1538-4357/ad0461

Gedalin, M. (2023c). Rankine-Hugoniot relations in turbulent shocks. *Frontiers in Physics*, *11*, 1325995. https://doi.org/10.3389/fphy.2023.1325995

Gedalin, M. (2024). Electron scattering on small-scale electrostatic fields in the shock front. *Journal of Plasma Physics*, *90*(5), 905900509. https://doi.org/10.1017/S0022377824001223

Gedalin, M., Dröge, W., & Kartavykh, Y. Y. (2015). Scattering of high-energy particles at a collisionless shock front: Dependence on the shock angle. *The Astrophysical Journal*, *807*(2), 126. https://doi.org/10.1088/0004-637X/807/2/126

Gedalin, M., Dröge, W., & Kartavykh, Y. Y. (2016). Dependence of the spectrum of shock-accelerated ions on the dynamics at the shock crossing. *Physical Review Letters*, *117*(27), 275101. https://doi.org/10.1103/PhysRevLett.117.275101

Gedalin, M., Friedman, Y., & Balikhin, M. (2015). Collisionless relaxation of downstream ion distributions in low-Mach number shocks. *Physics of Plasmas*, *22*(7), 072301. https://doi.org/10.1063/1.4926452

Gedalin, M., & Ganushkina, N. (2022). Implications of weak rippling of the shock ramp on the pattern of the electromagnetic field and ion distributions. *Journal of Plasma Physics*, *88*(3), 905880301. https://doi.org/10.1017/S0022377822000356

Gedalin, M., Golan, M., Vink, J., Ganushkina, N., & Balikhin, M. (2023). Electron heating in shocks: Statistics and comparison. *Journal of Geophysical Research: Space Physics*, *128*(9), e2023JA031627. https://doi.org/10.1029/2023JA031627

Gedalin, M., Golbraikh, E., Russell, C. T., & Dimmock, A. P. (2022). Theory helps observations: Determination of the shock Mach number and scales from magnetic measurements. *Frontiers in Physics*, *10*, 11. https://doi.org/10.3389/fphy.2022.852720

Gedalin, M., Kushinsky, Y., & Balikhin, M. (2015). Profile of a low-Mach-number shock in two-fluid plasma theory. *Annales Geophysicae*, *33*(8), 1011–1017. https://doi.org/10.5194/angeo-33-1011-2015

Gedalin, M., & Roytershteyn, V. (2024). Self-organization of collisionless shocks: From a laminar profile to a rippled time-dependent structure. *Journal of Plasma Physics*, *90*(6), 905900606. https://doi.org/10.1017/S0022377824001429

Gedalin, M., Russell, C. T., & Dimmock, A. P. (2021). Shock Mach number estimates using incomplete measurements. *Journal of Geophysical Research: Space Physics*, *126*(10), e2021JA029519. https://doi.org/10.1029/2021JA029519

Gedalin, M., & Zilbersher, D. (1995). Non-diagonal ion pressure in nearly-perpendicular collisionless shocks. *Geophysical Research Letters*, *22*(2), 3279–3282. https://doi.org/10.1029/95GL03284

Ghavamian, P., Laming, J. M., & Rakowski, C. E. (2007). A physical relationship between electron-proton temperature equilibration and Mach number in fast collisionless shocks. *The Astrophysical Journal*, *654*(1), L69–L72. https://doi.org/10.1086/510740

Ghavamian, P., Schwartz, S. J., Mitchell, J., Masters, A., & Laming, J. M. (2013). Electron-ion temperature equilibration in collisionless shocks: The Supernova Remnant-solar wind connection. *Space Science Reviews*, *178*(2), 633–663. https://doi.org/10.1007/s11214-013-9999-0

Giacalone, J., & Jokipii, J. R. (2006). Shock acceleration of high-energy cosmic rays: The importance of the magnetic-field angle. *Journal of Physics Conference Series*, *47*, 160–167. https://doi.org/10.1088/1742-6596/47/1/020

Gingell, I., Schwartz, S. J., Burgess, D., Johlander, A., Russell, C. T., Burch, J. L., et al. (2017). MMS observations and hybrid simulations of surface ripples at a marginally quasi-parallel shock. *Journal of Geophysical Research: Space Physics*, *77*(16), 11003–11017. https://doi.org/10.1002/2017JA024538

Golan, M., & Gedalin, M. (2025). Observations of persistent downstream magnetic oscillations at the Earth bow shock. *Journal of Geophysical Research: Space Physics*, *130*(9), e2025JA034321. https://doi.org/10.1029/2025JA034321

Goodrich, C. C., & Scudder, J. D. (1984). The adiabatic energy change of plasma electrons and the frame dependence of the cross-shock potential at collisionless magnetosonic shock waves. *Journal of Geophysical Research*, *89*(A8), 6654–6662. https://doi.org/10.1029/JA089iA08p06654

Goodrich, K. A., Ergun, R., Schwartz, S. J., Wilson, L. B., Newman, D., Wilder, F. D., et al. (2018). MMS observations of electrostatic waves in an oblique shock crossing. *Journal of Geophysical Research: Space Physics*, *123*(1), 9430–9442. https://doi.org/10.1029/2018JA025830

Gosling, J. T., & Thomsen, M. F. (1985). Specularly reflected ions, shock foot thicknesses, and shock velocity determinations in space. *Journal of Geophysical Research*, *90*(A10), 9893–9896. https://doi.org/10.1029/JA090iA10p09893

Gosling, J. T., Thomsen, M. F., Bame, S. J., Feldman, W. C., Paschmann, G., & Sckopke, N. (1982). Evidence for specularly reflected ions upstream from the quasi-parallel bow shock. *Geophysical Research Letters*, *9*(12), 1333–1336. https://doi.org/10.1029/GL009i012p01333

Graham, D. B., & Khotyaintsev, Y. V. (2025). The structure and kinetic ion behavior of low Mach number shocks. *Journal of Geophysical Research: Space Physics*, *130*(5), e2024JA033283. https://doi.org/10.1029/2024JA033283

Granit, G., & Gedalin, M. (2018). Whistler precursor and intrinsic variability of quasi-perpendicular shocks. *Journal of Plasma Physics*, *84*(1), 905840113. https://doi.org/10.1017/S0022377818000107

Greco, E., Vink, J., Ellien, A., & Ferrigno, C. (2023). Jitter radiation as an alternative mechanism for the nonthermal X-ray emission of Cassiopeia A. *The Astrophysical Journal*, *956*(2), 116. https://doi.org/10.3847/1538-4357/acf567

Greenstadt, E. W., Scarf, F. L., Russell, C. T., Formisano, V., & Neugebauer, M. (1975). Structure of the quasi-perpendicular laminar bow shock. *Journal of Geophysical Research*, *80*(4), 502–514. https://doi.org/10.1029/JA080i004p00502

Gustafsson, G., André, M., Carozzi, T., Eriksson, A. I., Fälthammar, C.-G., Grard, R., et al. (2001). First results of electric field and density observations by Cluster EFW based on initial months of operation. *Annales Geophysicae*, *19*(10/12), 1219–1240. https://doi.org/10.5194/angeo-19-1219-2001

Hanson, E. L. M., Agapitov, O. V., Mozer, F. S., Krasnoselskikh, V., Bale, S. D., Avanov, L., et al. (2019). Cross-shock potential in rippled versus planar quasi-perpendicular shocks observed by MMS. *Geophysical Research Letters*, *46*(5), 2381–2389. https://doi.org/10.1029/2018GL080240

Hellinger, P., Trávnícek, P., & Matsumoto, H. (2002). Reformation of perpendicular shocks: Hybrid simulations. *Geophysical Research Letters*, *29*(24), 4. https://doi.org/10.1029/2002GL015915

Hobara, Y., Balikhin, M., Krasnoselskikh, V., Gedalin, M., & Yamagishi, H. (2010). Statistical study of the quasi-perpendicular shock ramp widths. *Journal of Geophysical Research*, *115*(A11), A11106. https://doi.org/10.1029/2010JA015659

Horbury, T. S., O'Brien, H., Carrasco Blazquez, I., Bendyk, M., Brown, P., Hudson, R., et al. (2020). The Solar Orbiter magnetometer. *Astronomy & Astrophysics*, *642*, A9. https://doi.org/10.1051/0004-6361/201937257

Jebaraj, I. C., Agapitov, O., Krasnoselskikh, V., Vuorinen, L., Gedalin, M., Choi, K.-E., et al. (2024). Acceleration of electrons and ions by an "almost" astrophysical shock in the heliosphere. *The Astrophysical Journal Letters*, *968*(1), L8. https://doi.org/10.3847/2041-8213/ad4daa

Jebaraj, I. C., Agapitov, O. V., Gedalin, M., Vuorinen, L., Miceli, M., Cohen, C. M. S., et al. (2024). Direct measurements of synchrotron-emitting electrons at near-Sun shocks. *The Astrophysical Journal Letters*, *976*(1), L7. https://doi.org/10.3847/2041-8213/ad8eb8

Johlander, A., Khotyaintsev, Y. V., Dimmock, A. P., Graham, D. B., & Lalti, A. (2023). Electron heating scales in collisionless shocks measured by MMS. *Geophysical Research Letters*, *50*(5), e2022GL100400. https://doi.org/10.1029/2022GL100400

Johlander, A., Schwartz, S. J., Vaivads, A., Khotyaintsev, Y. V., Gingell, I., Peng, I. B., et al. (2016). Rippled quasiperpendicular shock observed by the magnetospheric multiscale spacecraft. *Physical Review Letters*, *117*(16), 165101. https://doi.org/10.1103/PhysRevLett.117.165101

Johlander, A., Vaivads, A., Khotyaintsev, Y. V., Gingell, I., Schwartz, S. J., Giles, B. L., et al. (2018). Shock ripples observed by the MMS spacecraft: Ion reflection and dispersive properties. *Plasma Physics and Controlled Fusion*, *60*(12), 125006. https://doi.org/10.1088/1361-6587/aae920

Jokipii, J. R. (1966a). A model of Fermi acceleration at shock fronts with an application to the Earth's bow shock. *The Astrophysical Journal*, *143*, 961. https://doi.org/10.1086/148571

Jokipii, J. R. (1966b). Pitch-angle dependence of first-order Fermi acceleration at shock fronts. *The Astrophysical Journal*, *145*, 616. https://doi.org/10.1086/148800

Kamaletdinov, S. R., Vasko, I. Y., & Artemyev, A. V. (2024). Nonlinear electron scattering by electrostatic waves in collisionless shocks. *Journal of Plasma Physics*, *90*(2), 905900201. https://doi.org/10.1017/S0022377824000217

Kamaletdinov, S. R., Vasko, I. Y., Artemyev, A. V., Wang, R., & Mozer, F. S. (2022). Quantifying electron scattering by electrostatic solitary waves in the Earth's bow shock. *Physics of Plasmas*, *29*(8), 082301. https://doi.org/10.1063/5.0097611

Kasper, J. C., Abiad, R., Austin, G., Balat-Pichelin, M., Bale, S. D., Belcher, J. W., et al. (2016). Solar wind electrons alphas and protons (SWEAP) investigation: Design of the solar wind and coronal plasma instrument suite for solar probe plus. *Space Science Reviews*, *204*(1–4), 131–186. https://doi.org/10.1007/s11214-015-0206-3

Katou, T., & Amano, T. (2019). Theory of stochastic shock drift acceleration for electrons in the shock transition region. *The Astrophysical Journal*, *874*(2), 119. https://doi.org/10.3847/1538-4357/ab0d8a

Kellogg, P. J. (1962). Flow of plasma around the Earth. *Journal of Geophysical Research*, *67*(10), 3805–3811. https://doi.org/10.1029/JZ067i010p03805

Kennel, C. F. (1987). Critical Mach numbers in classical magnetohydrodynamics. *Journal of Geophysical Research*, *92*(A12), 13427–13437. https://doi.org/10.1029/JA092iA12p13427

Kennel, C. F. (1988). Shock structure in classical magnetohydrodynamics. *Journal of Geophysical Research*, *93*(A8), 8545–8557. https://doi.org/10.1029/JA093iA08p08545

Kennel, C. F., Edmiston, J. P., & Hada, T. (1985). A quarter century of collisionless shock research. In *Collisionless shocks in the heliosphere: A tutorial review* (A87-25326 09-92) (Vol. 34, pp. 1–36).

Kennel, C. F., & Sagdeev, R. Z. (1967). Collisionless shock waves in high β plasmas: 2. *Journal of Geophysical Research*, *72*(1), 3327–3341. https://doi.org/10.1029/JZ072i013p03327

Kis, A., Scholer, M., Klecker, B., Möbius, E., Lucek, E. A., Rème, H., et al. (2004). Multi-spacecraft observations of diffuse ions upstream of Earth's bow shock. *Geophysical Research Letters*, *31*(2), 20801. https://doi.org/10.1029/2004GL020759

Krall, N. A., & Trivelpiece, A. W. (1973). Principles of plasma physics.

Krasnoselskikh, V., Balikhin, M., Walker, S. N., Schwartz, S., Sundkvist, D., Lobzin, V., et al. (2013). The dynamic quasiperpendicular shock: Cluster discoveries. *Space Science Reviews*, *178*(2), 535–598. https://doi.org/10.1007/s11214-013-9972-y

Krasnoselskikh, V. V. (1985). Nonlinear motions of a plasma across a magnetic field. *Soviet Physics Journal of Experimental and Theoretical Physics*, *62*, 282.

Krasnoselskikh, V. V., Lembège, B., Savoini, P., & Lobzin, V. V. (2002). Nonstationarity of strong collisionless quasiperpendicular shocks: Theory and full particle numerical simulations. *Physics of Plasmas*, *9*(4), 1192–1209. https://doi.org/10.1063/1.1457465

Kruparova, O., Krupar, V., Šafránková, J., Nemecek, Z., Maksimovic, M., Santolík, O., et al. (2019). Statistical survey of the terrestrial bow shock observed by the Cluster spacecraft. *Journal of Geophysical Research: Space Physics*, *124*(3), 1539–1547. https://doi.org/10.1029/2018JA026272

Krymskii, G. F. (1977). A regular mechanism for the acceleration of charged particles on the front of a shock wave. *Soviet Physics - Doklady*, *22*, 327.

Kucharek, H., Möbius, E., Scholer, M., Mouikis, C., Kistler, L. M., Horbury, T., et al. (2004). On the origin of field-aligned beams at the quasi-perpendicular bow shock: Multi-spacecraft observations by Cluster. *Annales Geophysicae*, *22*(7), 2301–2308. https://doi.org/10.5194/angeo-22-2301-2004

Kucharek, H., & Scholer, M. (1991). Origin of diffuse superthermal ions at quasi-parallel supercritical collisionless shocks. *Journal of Geophysical Research*, *96*(A12), 21195–21205. https://doi.org/10.1029/91JA02321

Lalti, A., Khotyaintsev, Y. V., Dimmock, A. P., Johlander, A., Graham, D. B., & Olshevsky, V. (2022). A database of MMS bow shock crossings compiled using machine learning. *Journal of Geophysical Research: Space Physics*, *127*(8), e2022JA030454. https://doi.org/10.1029/2022JA030454

Lalti, A., Khotyaintsev, Y. V., Graham, D. B., Vaivads, A., Steinvall, K., & Russell, C. T. (2022). Whistler waves in the foot of quasi-perpendicular supercritical shocks. *Journal of Geophysical Research: Space Physics*, *127*(5), e2021JA029969. https://doi.org/10.1029/2021JA029969

Lee, M. A., Shapiro, V. D., & Sagdeev, R. Z. (1996). Pickup ion energization by shock surfing. *Journal of Geophysical Research*, *101*(A3), 4777–4789. https://doi.org/10.1029/95JA03570

Lefebvre, B., Seki, Y., Schwartz, S. J., Mazelle, C., & Lucek, E. A. (2009). Reformation of an oblique shock observed by Cluster. *Journal of Geophysical Research*, *114*(A), A11107. https://doi.org/10.1029/2009JA014268

Lembège, B., & Savoini, P. (1992). Nonstationarity of a two-dimensional quasiperpendicular supercritical collisionless shock by self-reformation. *Physics of Fluids B: Plasma Physics*, *4*(11), 3533–3548. https://doi.org/10.1063/1.860361

Lepping, R. P., Acũna, M. H., Burlaga, L. F., Farrell, W. M., Slavin, J. A., Schatten, K. H., et al. (1995). The WIND magnetic field investigation. *Space Science Reviews*, *71*(1–4), 207–229. https://doi.org/10.1007/BF00751330

Leroy, M. M. (1984). Computer simulations of collisionless shock waves. *Advances in Space Research*, *4*(2–3), 231–243. https://doi.org/10.1016/0273-1177(84)90317-X

Leroy, M. M., Winske, D., Goodrich, C. C., Wu, C. S., & Papadopoulos, K. (1982). The structure of perpendicular bow shocks. *Journal of Geophysical Research*, *87*(A7), 5081–5094. https://doi.org/10.1029/JA087iA07p05081

Li, X., Lewis, H. R., LaBelle, J., Phan, T. D., & Treumann, R. A. (1995). Characteristics of the ion pressure tensor in the Earth's magnetosheath. *Geophysical Research Letters*, *22*(6), 667–670. https://doi.org/10.1029/95GL00005

Lindqvist, P.-A., Olsson, G., Torbert, R. B., King, B., Granoff, M., Rau, D., et al. (2016). The spin-plane double probe electric field instrument for MMS. *Space Science Reviews*, *199*(1–4), 137–165. https://doi.org/10.1007/s11214-014-0116-9

Liu, T. Z., Hao, Y., Wilson III, L. B., Turner, D. L., & Zhang, H. (2021). Magnetospheric multiscale observations of Earth's oblique bow shock reformation by foreshock ultralow-frequency waves. *Geophysical Research Letters*, *48*(2), e2020GL091184. https://doi.org/10.1029/2020GL091184

Livesey, W. A., Kennel, C. F., & Russell, C. T. (1982). ISEE-1 and -2 observations of magnetic field strength overshoots in quasi-perpendicular bow shocks. *Geophysical Research Letters*, *9*(9), 1037–1040. https://doi.org/10.1029/GL009i009p01037

Lobzin, V. V., Krasnoselskikh, V. V., Bosqued, J.-M., Pinçon, J.-L., Schwartz, S. J., & Dunlop, M. (2007). Nonstationarity and reformation of high-Mach-number quasiperpendicular shocks: Cluster observations. *Geophysical Research Letters*, *34*(5), 05107. https://doi.org/10.1029/2006GL029095

Lobzin, V. V., Krasnoselskikh, V. V., Musatenko, K., & Dudok de Wit, T. (2008). On nonstationarity and rippling of the quasiperpendicular zone of the Earth bow shock: Cluster observations. *Annales Geophysicae*, *26*(9), 2899–2910. https://doi.org/10.5194/angeo-26-2899-2008

Lowe, R. E., & Burgess, D. (2003). The properties and causes of rippling in quasi-perpendicular collisionless shock fronts. *Annales Geophysicae*, *21*(3), 671–679. https://doi.org/10.5194/angeo-21-671-2003

Luhmann, J. G., Curtis, D. W., Schroeder, P., McCauley, J., Lin, R. P., Larson, D. E., et al. (2008). STEREO IMPACT investigation goals, measurements, and data products overview. *Space Science Reviews*, *136*(1–4), 117–184. https://doi.org/10.1007/s11214-007-9170-x

Maksimovic, M., Bale, S. D., Chust, T., Khotyaintsev, Y., Krasnoselskikh, V., Kretzschmar, M., et al. (2020). The solar orbiter radio and plasma waves (RPW) instrument. *Astronomy & Astrophysics*, *642*, A12. https://doi.org/10.1051/0004-6361/201936214

Malaspina, D. M., Ergun, R. E., Bolton, M., Kien, M., Summers, D., Stevens, K., et al. (2016). The Digital Fields Board for the FIELDS instrument suite on the Solar Probe Plus mission: Analog and digital signal processing. *Journal of Geophysical Research: Space Physics*, *121*(6), 5088–5096. https://doi.org/10.1002/2016JA022344

Malkov, M., & Völk, H. (1998). Diffusive ion acceleration at shocks: The problem of injection. *Advances in Space Research*, *21*(4), 551–554. https://doi.org/10.1016/s0273-1177(97)00961-7

Malkov, M. A., Diamond, P. H., & Sagdeev, R. Z. (2010). On the structure and scale of cosmic ray modified shocks. *Plasma Physics and Controlled Fusion*, *52*(12), 124006. https://doi.org/10.1088/0741-3335/52/12/124006

Marcowith, A., Bret, A., Bykov, A., Dieckman, M. E., Drury, L. O., Lembège, B., et al. (2016). The microphysics of collisionless shock waves. *Reports on Progress in Physics*, *79*(4), 046901. https://doi.org/10.1088/0034-4885/79/4/046901

Markevitch, M., & Vikhlinin, A. (2007). Shocks and cold fronts in galaxy clusters. *Physics Reports*, *443*, 1–53. https://doi.org/10.1016/j.physrep.2007.01.001

Marshall, W. (1956). Structure of magnetohydrodynamic shock wave in a plasma of infinite conductivity. *Physical Review*, *103*(6), 1900. https://doi.org/10.1103/PhysRev.103.1900

Masters, A., Slavin, J. A., Dibraccio, G. A., Sundberg, T., Winslow, R. M., Johnson, C. L., et al. (2013). A comparison of magnetic overshoots at the bow shocks of Mercury and Saturn. *Journal of Geophysical Research: Space Physics*, *118*(7), 4381–4390. https://doi.org/10.1002/jgra.50428

Mazelle, C., Lembège, B., Morgenthaler, A., Meziane, K., Horbury, T. S., Génot, V., et al. (2010). Self-reformation of the quasi-perpendicular shock: CLUSTER observations. In *12th International Solar Wind Conference* (Vol. 1216, pp. 471–474). American Institute of Physics. https://doi.org/10.1063/1.3395905

Mazelle, C., Meziane, K., LeQuéau, D., Wilber, M., Eastwood, J., Rème, H., et al. (2003). Production of gyrating ions from nonlinear wave–particle interaction upstream from the Earth's bow shock: A case study from Cluster-CIS. *Planetary and Space Science*, *51*(12), 785–795. https://doi.org/10.1016/j.pss.2003.05.002

McComas, D. J., Bame, S. J., Barker, P., Feldman, W. C., Phillips, J. L., Riley, P., & Griffee, J. W. (1998). Solar wind electron proton alpha monitor (SWEPAM) for the Advanced Composition Explorer. *Space Science Reviews*, *86*(1–4), 563–612. https://doi.org/10.1023/A:1005040232597

McFadden, J. P., Carlson, C. W., Larson, D., Ludlam, M., Abiad, R., Elliott, B., et al. (2008). The THEMIS ESA plasma instrument and in-flight calibration. *Space Science Reviews*, *141*(1–4), 277–302. https://doi.org/10.1007/s11214-008-9440-2

Mellott, M. M., & Livesey, W. A. (1987). Shock overshoots revisited. *Journal of Geophysical Research*, *92*(A12), 13661–13665. https://doi.org/10.1029/JA092iA12p13661

Meziane, K., Lin, R., Larson, D., Mazelle, C., LeQueau, D., Parks, G. K., & Lepping, R. P. (2001). Three-dimensional observations of gyrating ion distributions far upstream from the Earth's bow shock and their association with low-frequency waves. *Journal of Geophysical Research*, *106*(A4), 5731–5742. https://doi.org/10.1029/2000ja900079

Meziane, K., Mazelle, C., D'Uston, C., Rème, H., Lin, R. P., Carlson, C. W., et al. (1997). WIND observation of gyrating-like ion distributions and low frequency waves upstream from the Earth's bow shock. *Advances in Space Research*, *20*(4–5), 703–706. https://doi.org/10.1016/S0273-1177(97)00459-6

Meziane, K., Wilber, M., Mazelle, C., LeQuéau, D., Kucharek, H., Lucek, E. A., et al. (2004). Simultaneous observations of field-aligned beams and gyrating ions in the terrestrial foreshock. *Journal of Geophysical Research*, *109*(A5), A05107. https://doi.org/10.1029/2003JA010374

Meziane, K., Wilber, M., Mazelle, C., Parks, G. K., & Hamza, A. M. (2004). A review of field-aligned beams observed upstream of the bow shock. In *AIP conference proceedings* (Vol. 781, No. 1, pp. 116–122). American Institute of Physics. https://doi.org/10.1063/1.2032683

Moebius, E., Scholer, M., Sckopke, N., Paschmann, G., & Luehr, H. (1987). The distribution function of diffuse ions and the magnetic field power spectrum upstream of earth's bow shock. *Geophysical Research Letters*, *14*, 681–684. https://doi.org/10.1029/GL014i007p00681

Mouhot, C., & Villani, C. (2011). On Landau damping. *Acta Mathematica*, *207*(1), 29–201. https://doi.org/10.1007/s11511-011-0068-9

Moullard, O., Burgess, D., Horbury, T. S., & Lucek, E. A. (2006). Ripples observed on the surface of the Earth's quasi-perpendicular bow shock. *Journal of Geophysical Research*, *111*(A), A09113. https://doi.org/10.1029/2005JA011594

Ness, N. F., Scearce, C. S., & Seek, J. B. (1964). Initial results of the imp 1 magnetic field experiment. *Journal of Geophysical Research*, *69*(17), 3531–3569. https://doi.org/10.1029/JZ069i017p03531

Neugebauer, M. (2013). Propagating shocks. *Space Science Reviews*, *176*(1–4), 125–132. https://doi.org/10.1007/s11214-010-9707-2

Neugebauer, M., & Giacalone, J. (2005). Multispacecraft observations of interplanetary shocks: Nonplanarity and energetic particles. *Journal of Geophysical Research*, *110*(A12), A12106. https://doi.org/10.1029/2005JA011380

Newbury, J. A., & Russell, C. T. (1996). Observations of a very thin collisionless shock. *Geophysical Research Letters*, *23*(7), 781–784. https://doi.org/10.1029/96GL00700

Newbury, J. A., Russell, C. T., & Gedalin, M. (1997). The determination of shock ramp width using the noncoplanar magnetic field component. *Geophysical Research Letters*, *24*(1), 1975–1978. https://doi.org/10.1029/97GL01977

Newbury, J. A., Russell, C. T., & Gedalin, M. (1998). The ramp widths of high-Mach-number, quasi-perpendicular collisionless shocks. *Journal of Geophysical Research*, *103*(A12), 29581–29594. https://doi.org/10.1029/1998JA900024

Ofman, L., Balikhin, M., Russell, C. T., & Gedalin, M. (2009). Collisionless relaxation of ion distributions downstream of laminar quasi-perpendicular shocks. *Journal of Geophysical Research*, *114*(A), 09106. https://doi.org/10.1029/2009JA014365

Ofman, L., & Gedalin, M. (2013). Rippled quasi-perpendicular collisionless shocks: Local and global normals. *Journal of Geophysical Research: Space Physics*, *118*(1), 5999–6006. https://doi.org/10.1002/2013JA018780

Ogilvie, K. W., Chornay, D. J., Fritzenreiter, R. J., Hunsaker, F., Keller, J., Lobell, J., et al. (1995). SWE, a comprehensive plasma instrument for the Wind spacecraft. *Space Science Reviews*, *71*(1–4), 55–77. https://doi.org/10.1007/BF00751326

Oka, M., Terasawa, T., Saito, Y., & Mukai, T. (2005). Field-aligned beam observations at the quasi-perpendicular bow shock: Generation and shock angle dependence. *Journal of Geophysical Research*, *110*(A), A05101. https://doi.org/10.1029/2004JA010688

Omidi, N., Desai, M., Russell, C. T., & Howes, G. G. (2021). High Mach number quasi-perpendicular shocks: Spatial versus temporal structure. *Journal of Geophysical Research: Space Physics*, *126*(9), e2021JA029287. https://doi.org/10.1029/2021JA029287

Owen, C. J., Bruno, R., Livi, S., Louarn, P., Al Janabi, K., Allegrini, F., et al. (2020). The Solar Orbiter Solar Wind Analyser (SWA) suite. *Astronomy & Astrophysics*, *642*, A16. https://doi.org/10.1051/0004-6361/201937259

Parker, E. N. (1958). Dynamics of the interplanetary gas and magnetic fields. *The Astrophysical Journal*, *128*, 664. https://doi.org/10.1086/146579

Paschmann, G., Sckopke, N., Bame, S. J., & Gosling, J. T. (1982). Observations of gyrating ions in the foot of the nearly perpendicular bow shock. *Geophysical Research Letters*, *9*, 881. https://doi.org/10.1029/GL009i008p00881

Paschmann, G., Sckopke, N., Papamastorakis, I., Asbridge, J. R., Bame, S. J., & Gosling, J. T. (1981). Characteristics of reflected and diffuse ions upstream from the Earth's bow shock. *Upstream Wave and Particle Workshop*, *86*(A6), 4355–4364. https://doi.org/10.1029/JA086iA06p04355

Patrick, R. M. (1959). High-speed shock waves in a magnetic annular shock tube. *The Physics of Fluids*, *2*(6), 589–598. https://doi.org/10.1063/1.1705959

Paul, J. W. M., Holmes, L. S., Parkinson, M. J., & Sheffield, J. (1965). Experimental observations on the structure of collisionless shock waves in a magnetized plasma. *Nature*, *208*(5006), 133–135. https://doi.org/10.1038/208133a0

Phillips, P. E., & Robson, A. E. (1972). Influence of reflected ions on the magnetic structure of a collisionless shock. *Physical Review Letters*, *29*(3), 154–157. https://doi.org/10.1103/PhysRevLett.29.154

Pollock, C., Moore, T., Jacques, A., Burch, J., Gliese, U., Omoto, T., et al. (2016). Fast plasma investigation for magnetospheric multiscale. *Space Science Reviews*, *199*(1–4), 331–406. https://doi.org/10.1007/s11214-016-0245-4

Pope, S. A. (2020). A survey of Venus shock crossings dominated by kinematic relaxation. *Journal of Geophysical Research: Space Physics*, *125*(1), A028256. https://doi.org/10.1029/2020JA028256

Pope, S. A., Gedalin, M., & Balikhin, M. A. (2018). Observations of very-low Mach number inner planet bow shocks during ICMEs. *20th EGU General Assembly*, *20*, 15975.

Pope, S. A., Gedalin, M., & Balikhin, M. A. (2019). The first direct observational confirmation of kinematic collisionless relaxation in very low Mach number shocks near the Earth. *Journal of Geophysical Research: Space Physics*, *124*(1), 1711–1725. https://doi.org/10.1029/2018JA026223

Ptuskin, V. S., Rogovaya, S. I., & Zirakashvili, V. N. (2009). Acceleration of ultra-high energy cosmic rays by galaxy cluster accretion shocks. *Bulletin of the Russian Academy of Sciences: Physics*, *73*(5), 552–554. https://doi.org/10.3103/S1062873809050050

Rakowski, C. E., Laming, J. M., & Ghavamian, P. (2008). The heating of thermal electrons in fast collisionless shocks: The integral role of cosmic rays. *The Astrophysical Journal*, *684*(1), 348–357. https://doi.org/10.1086/590245

Raymond, J. C., Ghavamian, P., Bohdan, A., Ryu, D., Niemiec, J., Sironi, L., et al. (2023). Electron–ion temperature ratio in astrophysical shocks. *The Astrophysical Journal*, *949*(2), 50. https://doi.org/10.3847/1538-4357/acc528

Rème, H., Aoustin, C., Bosqued, J. M., Dandouras, I., Lavraud, B., Sauvaud, J. A., et al. (2001). First multispacecraft ion measurements in and near the Earth's magnetosphere with the identical Cluster ion spectrometry (CIS) experiment. *Annales Geophysicae*, *19*(10/12), 1303–1354. https://doi.org/10.5194/angeo-19-1303-2001

Russell, C. T. (1988). Multipoint measurements of upstream waves. *Advances in Space Research*, *8*(9–10), 147–156. https://doi.org/10.1016/0273-1177(88)90125-1

Russell, C. T., & Alexander, C. J. (1984). Multiple spacecraft observations of interplanetary shocks: Shock-normal oscillations and their effects. *Advances in Space Research*, *4*(2–3), 277–282. https://doi.org/10.1016/0273-1177(84)90321-1

Russell, C. T., Anderson, B. J., Baumjohann, W., Bromund, K. R., Dearborn, D., Fischer, D., et al. (2016). The magnetospheric multiscale magnetometers. *Space Science Reviews*, *199*(1–4), 189–256. https://doi.org/10.1007/s11214-014-0057-3

Russell, C. T., Hoppe, M. M., & Livesey, W. A. (1982). Overshoots in planetary bow shocks. *Nature*, *296*(5852), 45–48. https://doi.org/10.1038/296045a0

Russell, C. T., Hoppe, M. M., Livesey, W. A., Gosling, J. T., & Bame, S. J. (1982). ISEE-1 and -2 observations of laminar bow shocks - Velocity and thickness. *Geophysical Research Letters*, *9*(10), 1171–1174. https://doi.org/10.1029/GL009i010p01171

Russell, C. T., Luhmann, J. G., Elphic, R. C., Southwood, D. J., Smith, M. F., & Johnstone, A. D. (1987). Upstream waves simultaneously observed by ISEE and UKS. *Journal of Geophysical Research*, *92*(A7), 7354–7362. https://doi.org/10.1029/JA092iA07p07354

Russell, C. T., Mellott, M. M., Smith, E. J., & King, J. H. (1983). Multiple spacecraft observations of interplanetary shocks: Four spacecraft determination of shock normals. *Journal of Geophysical Research*, *88*(A6), 4739–4748. https://doi.org/10.1029/JA088iA06p04739

Sagdeev, R. Z. (1966). Cooperative phenomena and shock waves in collisionless plasmas. *Reviews of Plasma Physics*, *4*, 23.

Sagdeev, R. Z. (1979). The 1976 Oppenheimer lectures: Critical problems in plasma astrophysics. II. Singular layers and reconnection. *Reviews of Modern Physics*, *51*(1), 11–20. https://doi.org/10.1103/RevModPhys.51.11

Sagdeev, R. Z., Kadomtsev, B., Rudakov, L., & Vedenov, A. (1958). Dynamics of rare plasma in a magnetic field. *Journal of Nuclear Energy*, *7*(3–4), 301. https://doi.org/10.1016/0891-3919(58)90182-7

Sagdeev, R. Z., & Kennel, C. F. (1991). Collisionless shock waves. *Scientific American*, *264*(4), 106–115. https://doi.org/10.1038/scientificamerican0491-106

Schaeffer, D. B., Everson, E. T., Bondarenko, A. S., Clark, S. E., Constantin, C. G., Winske, D., et al. (2015). Experimental study of subcritical laboratory magnetized collisionless shocks using a laser-driven magnetic piston. *Physics of Plasmas*, *22*(11), 113101. https://doi.org/10.1063/1.4934983

Schwartz, S. J. (1998). Shock and discontinuity normals, Mach numbers, and related parameters. In G. Paschmann & P. Daly (Eds.), *Analysis methods for multi-spacecraft data*, *ISSI Scientific Reports Series* (Vol. 1, pp. 249–270).

Schwartz, S. J., & Burgess, D. (1991). Quasi-parallel shocks - A patchwork of three-dimensional structures. *Geophysical Research Letters*, *18*(3), 373–376. https://doi.org/10.1029/91GL00138

Schwartz, S. J., Douglas, F. T., Thomsen, M. F., & Feldman, W. C. (1987). Electron dynamics and potential jump across slow mode shocks. *Journal of Geophysical Research*, *92*(A4), 3165–3174. https://doi.org/10.1029/JA092iA04p03165

Schwartz, S. J., Thomsen, M. F., Bame, S. J., & Stansberry, J. (1988). Electron heating and the potential jump across fast mode shocks. *Journal of Geophysical Research*, *93*(A11), 12923–12931. https://doi.org/10.1029/JA093iA11p12923

Sckopke, N., Paschmann, G., Bame, S. J., Gosling, J. T., & Russell, C. T. (1983). Evolution of ion distributions across the nearly perpendicular bow shock - Specularly and non-specularly reflected-gyrating ions. *Journal of Geophysical Research*, *88*(A8), 6121–6136. https://doi.org/10.1029/JA088iA08p06121

Sckopke, N., Paschmann, G., Brinca, A. L., Carlson, C. W., & Luehr, H. (1990). Ion thermalization in quasi-perpendicular shocks involving reflected ions. *Journal of Geophysical Research*, *95*(A5), 6337–6352. https://doi.org/10.1029/JA095iA05p06337

Scudder, J., Scudder, J. D., Aggson, T. L., Aggson, T., Mangeney, A., Lacombe, C., & Harvey, C. C. (1986). The resolved layer of a collisionless, high beta, supercritical, quasi-perpendicular shock wave. II - Dissipative fluid electrodynamics. *Journal of Geophysical Research*, *91*(A10), 11053–11073. https://doi.org/10.1029/JA091iA10p11053

Sen, H. K. (1956). Structure of a magnetohydrodynamic shock wave in a plasma of infinite conductivity. *Physical Review*, *102*(1), 5–11. https://doi.org/10.1103/PhysRev.102.5

Sharma, P., & Gedalin, M. (2023). Non-specular ion reflection at quasiperpendicular collisionless shock front. *Journal of Plasma Physics*, *89*(5), 905890505. https://doi.org/10.1017/S002237782300096X

Shi, X., Artemyev, A., Angelopoulos, V., Liu, T., & Zhang, X.-J. (2023). Evidence of electron acceleration via nonlinear resonant interactions with whistler-mode waves at foreshock transients. *The Astrophysical Journal*, *952*(1), 38. https://doi.org/10.3847/1538-4357/acd9ab

Shi, X., Tonoian, D. S., Artemyev, A. V., Zhang, X.-J., & Angelopoulos, V. (2023). Electron resonant interaction with whistler-mode waves around the Earth's bow shock I: The probabilistic approach. *Physics of Plasmas*, *30*(12), 122902. https://doi.org/10.1063/5.0172231

Skilling, J. (1975a). Cosmic ray streaming. I - Effect of Alfven waves on particles. *Monthly Notices of the Royal Astronomical Society*, *172*(3), 557–566. https://doi.org/10.1093/mnras/172.3.557

Skilling, J. (1975b). Cosmic ray streaming. II - Effect of particles on Alfven waves. *Monthly Notices of the Royal Astronomical Society*, *173*(2), 245–254. https://doi.org/10.1093/mnras/173.2.245

Skilling, J. (1975c). Cosmic ray streaming. III - Self-Consistent solutions. *Monthly Notices of the Royal Astronomical Society*, *173*(2), 255–269. https://doi.org/10.1093/mnras/173.2.255

Smith, C. W., L'Heureux, J., Ness, N. F., Acuña, M. H., Burlaga, L. F., & Scheifele, J. (1998). The ACE magnetic fields experiment. *Space Science Reviews*, *86*(1–4), 613–632. https://doi.org/10.1023/A:1005092216668

Sulaiman, A. H., Masters, A., & Dougherty, M. K. (2016). Characterization of Saturn's bow shock: Magnetic field observations of quasi-perpendicular shocks. *Journal of Geophysical Research: Space Physics*, *121*(5), 4425–4434. https://doi.org/10.1002/2016JA022449

Sulaiman, A. H., Masters, A., Dougherty, M. K., Burgess, D., Fujimoto, M., & Hospodarsky, G. B. (2015). Quasiperpendicular high Mach number shocks. *Physical Review Letters*, *115*(12), 125001. https://doi.org/10.1103/PhysRevLett.115.125001

Tatrallyay, M., Gevai, G., Apathy, I., Schwingenschuh, K., Zhang, T. L., Kotova, G. A., et al. (1997). Magnetic field overshoots in the Martian bow shock. *Journal of Geophysical Research*, *102*(A), 2157–2164. https://doi.org/10.1029/96JA00073

Tatrallyay, M., Luhmann, J. G., & Russell, C. T. (1984). Magnetic field overshoots in the Venus bow shock. *Advances in Space Research*, *4*, 283–286. https://doi.org/10.1016/0273-1177/84

Terasawa, T., Hada, T., Matsukiyo, S., Oka, M., Bamba, A., & Yamazaki, R. (2007). Shock modification by cosmic-ray-excited turbulences. *Progress of Theoretical Physics Supplement*, *169*, 146–149. https://doi.org/10.1143/PTPS.169.146

Thomsen, M., Stansberry, J., Bame, S., & Gosling, J. (1987). Strong electron heating at the Earth's bow shock. *Journal of Geophysical Research*, *92*, 10119–10124.

Thomsen, M. F., Gosling, J. T., Bame, S. J., Feldman, W. C., Paschmann, G., & Sckopke, N. (1983). Field-aligned ion beams upstream of the Earth's bow shock Evidence for a magnetosheath source. *Geophysical Research Letters*, *10*(12), 1207–1210. https://doi.org/10.1029/GL010i012p01207

Thomsen, M. F., Gosling, J. T., Bame, S. J., & Mellott, M. M. (1985). Ion and electron heating at collisionless shocks near the critical Mach number. *Journal of Geophysical Research*, *90*(A1), 137–148. https://doi.org/10.1029/JA090iA01p00137

Tidman, D. A. (1958). Structure of a shock wave in fully ionized hydrogen. *Physical Review*, *111*(6), 1439–1446. https://doi.org/10.1103/PhysRev.111.1439

Tiu, D., Cairns, I. H., Yuan, X., & Robinson, P. A. (2011). Evidence for reformation of the Uranian bow shock: Hybrid simulations and comparisons with Voyager data. *Journal of Geophysical Research*, *116*(A), A04228. https://doi.org/10.1029/2010JA016057

Toptyghin, I. N. (1980). Acceleration of particles by shocks in a cosmic plasma. *Space Science Reviews*, *26*(2), 157–213. https://doi.org/10.1007/BF00167370

Trattner, K. J., Fuselier, S. A., Schwartz, S. J., Kucharek, H., Burch, J. L., Ergun, R. E., et al. (2023). Ion acceleration at the quasi-parallel shock: The source distributions of the diffuse ions. *Journal of Geophysical Research: Space Physics*, *128*(2), e2022JA030631. https://doi.org/10.1029/2022JA030631

Trotta, D., Dimmock, A., Hietala, H., Blanco-Cano, X., Horbury, T. S., Vainio, R., et al. (2025). An overview of solar orbiter observations of interplanetary shocks in solar cycle 25. *The Astrophysical Journal Supplement Series*, *277*(1), 2. https://doi.org/10.3847/1538-4365/ada4a7

Turner, D. L., Wilson, L. B., Goodrich, K. A., Madanian, H., Schwartz, S. J., Liu, T. Z., et al. (2021). Direct multipoint observations capturing the reformation of a supercritical fast magnetosonic shock. *The Astrophysical Journal Letters*, *911*(2), L31. https://doi.org/10.3847/2041-8213/abec78

Vasko, I. Y., Mozer, F. S., Krasnoselskikh, V. V., Artemyev, A. V., Agapitov, O. V., Bale, S. D., et al. (2018). Solitary waves across supercritical quasi-perpendicular shocks. *Geophysical Research Letters*, *45*(1), 5809–5817. https://doi.org/10.1029/2018GL077835

Vasko, I. Y., Wang, R., Mozer, F. S., Bale, S. D., & Artemyev, A. V. (2020). On the nature and origin of bipolar electrostatic structures in the Earth's bow shock. *Frontiers in Physics*, *8*, 156. https://doi.org/10.3389/fphy.2020.00156

Vink, J. (2004). Shocks and particle acceleration in supernova remnants: Observational features. *Advances in Space Research*, *33*(4), 356–365. https://doi.org/10.1016/j.asr.2003.05.012

Wang, R., Vasko, I. Y., Mozer, F. S., Bale, S. D., Artemyev, A. V., Bonnell, J. W., et al. (2020). Electrostatic turbulence and Debye-scale structures in collisionless shocks. *The Astrophysical Journal Letters*, *889*(1), L9. https://doi.org/10.3847/2041-8213/ab6582

Wang, R., Vasko, I. Y., Mozer, F. S., Bale, S. D., Kuzichev, I. V., Artemyev, A. V., et al. (2021). Electrostatic solitary waves in the Earth's bow shock: Nature, properties, lifetimes, and origin. *Journal of Geophysical Research: Space Physics*, *126*(7), e2021JA029357. https://doi.org/10.1029/2021JA029357

Webb, G. M., Axford, W. I., & Terasawa, T. (1983). On the drift mechanism for energetic charged particles at shocks. *The Astrophysical Journal*, *270*, 537–553. https://doi.org/10.1086/161146

Wilson III, L. B., Koval, A., Szabo, A., Stevens, M. L., Kasper, J. C., Cattell, C. A., & Krasnoselskikh, V. V. (2017). Revisiting the structure of low-Mach number, low-beta, quasi-perpendicular shocks. *Journal of Geophysical Research: Space Physics*, *81*(4), 2097–9133. https://doi.org/10.1002/2017JA024352

Woods, L. (1971). On double-structured, perpendicular, magneto-plasma shock waves. *Plasma Physics*, *13*(4), 289–302. https://doi.org/10.1088/0032-1028/13/4/302

Woods, L. C. (1969). On the structure of collisionless magneto-plasma shock waves at super-critical Alfvén-Mach numbers. *Journal of Plasma Physics*, *3*(3), 435–447. https://doi.org/10.1017/S0022377800004517

Yuan, X., Cairns, I. H., Trichtchenko, L., Rankin, R., & Danskin, D. W. (2009). Confirmation of quasi-perpendicular shock reformation in two-dimensional hybrid simulations. *Geophysical Research Letters*, *36*(5), L05103. https://doi.org/10.1029/2008GL036675

Zank, G. P., Pauls, H. L., Cairns, I. H., & Webb, G. M. (1996). Interstellar pickup ions and quasi-perpendicular shocks: Implications for the termination shock and interplanetary shocks. *Journal of Geophysical Research*, *101*(A), 457–478. https://doi.org/10.1029/95JA02860